BEC preprints 2026.3
https://doi.org/10.26124/becprep.2025-0007.v2
Open Access

# Lower mitochondrial calcium uptake capacity than calcium retention capacity in the presence and absence of cyclosporin A

Cristiane Cecatto, Luiza Helena Daltro Cardoso, Mateus Grings, Erich Gnaiger

Oroboros Instruments GmbH, Innsbruck, Austria
Corresponding authors: cristiane.cecatto@oroboros.at; erich.gnaiger@oroboros.at

**Received** v1 2025-07-16; v2 2026-07-14 – **Online** 2026-07-21

**Cite**
Cecatto C, Cardoso LHD, Grings M, Gnaiger E (2026) Lower mitochondrial calcium uptake capacity than calcium retention capacity in the presence and absence of cyclosporin A. BEC preprints 2026.3. https://doi.org/10.26124/becprep.2025-0007.v2

**Keywords**
calcium; mitochondria; mitochondrial permeability transition; fluorescence; respiration; calcium green; high-resolution respirometry

## Summary

**Mitochondrial calcium homeostasis impacts on calcium-dependent cellular bioenergetics and health. Mitochondria contribute to the buffering of cytosolic calcium levels by uptake and release, or storage of osmotically inactive calcium phosphates in the mitochondrial matrix. Defective calcium homeostasis causes bioenergetic stress, cell death, and diseases. Since the interplay between $Ca^{2+}$ dynamics and oxidative phosphorylation is well recognized, mitochondrial calcium retention capacity is frequently measured as the amount of calcium titrated up to a threshold, when calcium uptake is reversed and permeability transition triggers the release of calcium, disruption of ion balance, dyscoupling, and inhibition of respiration. This is accompanied by leakage into the cytosolic space of signaling molecules such as cytochrome *c*. We measured extramitochondrial $[Ca^{2+}]$ using Calcium Green™-5N (CaG) simultaneously with high-resolution respirometry. The respiration medium MiRCa containing CaG did not impair respiration of isolated mouse liver mitochondria. $Ca^{2+}$ uptake was incomplete as shown by the merely partial decline of $[Ca^{2+}]$ in the medium after initial $[Ca^{2+}]$ titrations and final titrations prior to permeability transition. Consequently, $Ca^{2+}$ uptake capacity, corrected for the increase of $[Ca^{2+}]$ in the medium, was 45 % of the conventionally defined $Ca^{2+}$ retention capacity in controls and 55 % in the presence of cyclosporin A. Our results suggest that $Ca^{2+}$ retention capacities depend on experimental mitochondrial concentration, require critical evaluation, and should be replaced by $Ca^{2+}$ uptake capacities properly corrected for increased extramitochondrial calcium concentrations.**

## 1. Introduction

Mitochondria are central to cellular bioenergetics, primarily through their role in oxidative phosphorylation (OXPHOS). Beyond energy transformation, they play a crucial role in maintaining cellular calcium homeostasis by sequestering cytosolic calcium ions ($Ca^{2+}$). $Ca^{2+}$ is a pivotal and ubiquitous second messenger in various cellular signaling pathways (1-3). Mitochondrial $Ca^{2+}$ homeostasis is linked to cell survival and cell death. Excessive mitochondrial $Ca^{2+}$ accumulation initiates apoptosis, necrosis, or autophagy (4, 5). At lower concentrations, $Ca^{2+}$ activates pyruvate dehydrogenase phosphatase, oxoglutarate dehydrogenase, NAD-isocitrate dehydrogenase, mitochondrial glycerol phosphate dehydrogenase, and $F_1$-$F_O$-ATPase (6-8). The regulatory or pathological impact on oxidative phosphorylation depends on the $Ca^{2+}$ concentration (9, 10).

$Ca^{2+}$ is released from intracellular stores in the endoplasmic or sarcoplasmic reticulum (ER/SR) in response to diverse signaling mechanisms (1). After the signaling event, $Ca^{2+}$ is removed from the cytoplasm, with mitochondria playing a central role in maintaining cellular $Ca^{2+}$ homeostasis (11, 12). Pathological conditions can lead to $Ca^{2+}$ overload, which is potentially lethal to the cell if not properly regulated.

$Ca^{2+}$ uptake through the mitochondrial outer membrane is mediated by the voltage-dependent anion channel (VDAC), while transport across the mitochondrial inner membrane (mtIM) into the matrix is primarily mediated by the mitochondrial calcium uniporter (MCU) (13, 14). Transport by the MCU is electrogenic, driven by the mitochondrial membrane potential (mtMP) (5). The balance of matrix $Ca^{2+}$ concentration is maintained by $Ca^{2+}$ antiporters, including the mitochondrial $Na^+/Ca^{2+}/Li^+$ exchanger (NCLX) and the $H^+/Ca^{2+}$ exchanger, depending on tissue type (3).

Once inside the mitochondria, $Ca^{2+}$ forms phosphate-precipitates. Excessive uptake or impairment of the efflux system lead to mitochondrial $Ca^{2+}$ overload causing $Ca^{2+}$ release upon mitochondrial permeability transition (mtPT) (15). Prolonged opening of the permeability transition pore causes mtIM depolarization and mitochondrial swelling, and ultimately cell death (3, 16). Besides $Ca^{2+}$ as an essential permissive agent, mtPT is controlled by the protonmotive force and desensitized by Cyclosporin A (CsA). CsA is frequently used *in vitro* to evaluate the involvement of mtPT in pathological conditions (17-20). Both ATP and ADP are identified as mtPT inhibitors (21). Physiologically relevant concentrations of these adenylates and particularly ATP are, therefore, omitted in many studies on the nature of the mtPT pore.

Transient or flickering mtPT impacts on $Ca^{2+}$ release from mitochondria, preventing $Ca^{2+}$ overload. It regulates reactive oxygen species signaling, life span, cellular differentiation and is involved in rapid alterations of mitochondrial bioenergetics (16).

Cyclophilin D (CypD), a mitochondrial matrix peptidyl prolyl cis–trans isomerase, is a well-described protein involved in regulation of the mtPT pore. CsA binds to the

active site of CypD and thus desensitizes mtPT. CypD interacts with both the adenine nucleotide translocator and ATP synthase (22). The molecular nature and structure of the mtPT pore is a matter of debate (23, 24). In the absence of ATP, the adenine nucleotide translocator and ATP synthase cooperate as structural units in the regulation of mtPT (22). Several proteins — such as the phosphate carrier, VDAC, and hexokinase — may act as modulators of the mtPT pore. Multiple forms of the mtPT pore exist with different molecular composition and conductance (25).

$Ca^{2+}$ movements can be measured using a $Ca^{2+}$ fluorescent probe. A widely applied method uses the visible light-excitable $Ca^{2+}$ indicator Invitrogen™ Calcium Green™-5N (CaG), which is a membrane-impermeant potassium salt and therefore can be dissolved in water. It has lower buffering capacity for intracellular $Ca^{2+}$ compared to high-affinity dyes. In assays with isolated mitochondria or permeabilized cells, it enables to investigate the extramitochondrial $Ca^{2+}$ concentration and allows for tracking rapid $Ca^{2+}$-release kinetics (26). The results of this assay are frequently reported as calcium retention capacity (CaRC), calculated by summing up the $Ca^{2+}$ added until onset of mtPT. In principle, $Ca^{2+}$ measurement is irrelevant to obtain the CaRC, since mtPT can be observed by measurement of respiration, swelling or mtMP, although the latter is not a specific indicator (27). CaRC is higher than calcium uptake capacity (CaUC), which is the amount of $Ca^{2+}$ actually taken up by the mitochondria. This requires correction for the measured amount of accumulation of extramitochondrial $Ca^{2+}$ as analyzed in the present study.

While CaG is commonly used in spectrofluorimetry, its application in simultaneous assessments of mitochondrial respiration and calcium dynamics warrants further exploration. Monitoring mitochondrial respiration simultaneously with $Ca^{2+}$ uptake and retention/release advances the understanding of how $Ca^{2+}$ homeostasis and its dysregulation impact energy metabolism. Despite the critical interplay between mitochondrial calcium uptake and respiration, few studies have measured these parameters simultaneously (28-33).

The composition of incubation media affects CaRC, complicating comparison between studies (25). Some fluorescent dyes affect respiration (34, 35). We introduce a method to concurrently assess mitochondrial $Ca^{2+}$ dynamics and respiratory function in isolated mitochondria and permeabilized cells, with the development of a medium appropriate for both measurements. Our results highlight the importance of calculating the $Ca^{2+}$ actually taken up by the mitochondria (CaUC) up to mtPT, in contrast to merely summing up the $Ca^{2+}$ titrations to the point of mtPT (CaRC).

## 2. Experimental procedures

### Reagents and media

Calcium Green™-5N, a cell impermeant hexapotassium salt, was obtained from Invitrogen™ (Waltham, USA; cat. Nº C3737), with the standard $K_d$ given as ~14 µM (26). From Sigma Aldrich (Burlington, USA): Antimycin A (cat. Nº A8674), ATP (disodium salt hydrate, cat. Nº A2383, for BIOPS), ATP (disodium salt hydrate, cat. Nº

A26209, for ATP titration), BSA (fatty acid-free, cat. Nº A6003), $CaCO_3$ (calcium carbonate, cat. Nº C4830), $CaCl_2$ (calcium chloride, cat. Nº 21114), CCCP (carbonyl cyanide 3-chlorophenylhydrazone carbonate, cat. Nº C2759), cytochrome *c* (cat. Nº C7752), cyclosporin A (cat. Nº 30024), digitonin (cat. Nº D5628), DL-dithiothreitol (cat. Nº D0632), DMSO (cat. Nº 276855), $Na_2EDTA$ (disodium salt dihydrate, cat. Nº E1644), EGTA (cat. Nº E4378), glutamate (L-glutamic acid monosodium salt hydrate, cat. Nº G1626), HEPES (cat. Nº H7523), imidazole (cat. Nº 56750), malate (cat. Nº M1000), oligomycin (cat. Nº O4876), KCl (potassium chloride, cat. Nº 60130), $KH_2PO_4$ (potassium dihydrogen phosphate, cat. Nº P5655), KOH (potassium hydroxide, cat. Nº P1767), MES hydrate (cat. Nº M8250), $Na_2$-phosphocreatine (cat. Nº P7936), pyruvate (sodium salt, cat. Nº P2256), rotenone (cat. Nº R8875), succinate (sodium succinate dibasic hexahydrate, cat. Nº S2378), sucrose (cat. Nº S7903), taurine (cat. Nº T0625) and Tris (cat. Nº 252859). ADP (adenosine 5'-diphosphate, potassium salt, cat. Nº 117105) was acquired from Millipore (Burlington, USA), $MgCl_2 \cdot 6H_2O$ (magnesium chloride hexahydrate, cat. Nº LC-5041) from Labochem International (Athens, Greece), HCl (hydrochloric acid, cat. Nº 2315957) from Aurelio (Görlitz, Germany). Ethanol 99.9 % (CL0005055000) obtained from Bartelt, Graz, Austria and deionized ultra-pure water (prepared by Ultra ClearTM TP UV UF TM; Evoqua Water Technologies, Pittsburgh, USA) were used to prepare all solutions.

ADP 500 mM with 300 mM $MgCl_2$: 501.3 mg ADP was dissolved in 1.2 mL $H_2O$; pH was neutralized with 5 M KOH; 122.0 mg $MgCl_2 \cdot 6\ H_2O$ was added, pH was adjusted to 7 at room temperature (RT). ADP 15 mM for calcium uptake measurements was prepared by further dilution with $H_2O$.

ATP 200 mM: 1.1023 g ATP was dissolved in $H_2O$; pH was neutralized to 6.9 with KOH on ice. The volume was adjusted to 10 mL with $H_2O$.

Calcium chloride ($CaCl_2$) 10 mM: prepared fresh on every experimental day from the 1 M commercial solution, diluted with $H_2O$.

CaG 1 mM: prepared by dissolving 500 µg of Calcium Green™ in 419 µL $H_2O$, protected from light and aliquoted for storage.

Cyclosporin A (CsA) 400 µM: 1 mg of CsA was dissolved in 2.11 mL of ethanol abs.

Cytochrome *c* 4 mM: 50 mg cytochrome *c* was added to 1 mL $H_2O$ and aliquoted for storage.

Digitonin 8.1 mM: 10 mg of digitonin was dissolved in 1 mL of DMSO.

EGTA 20 mM: was prepared in $H_2O$, and the pH was adjusted to approximately 7 at RT with KOH to complete dissolution.

Glutamate 2 M: 1.691 g glutamate was dissolved with 4 mL $H_2O$. After pH adjustment to 7.0 with KOH at RT, the final volume was adjusted to 5 mL.

Oligomycin 5 mM: 4 mg oligomycin dissolved in 1 mL ethanol in a glass vial. A 0.01 mM solution was diluted with ethanol from the 5 mM. Aliquots were stored in glass vials.

BIOPS: 10 mM $Ca^{2+}$-EGTA - 0.1 µM free $Ca^{2+}$, 20 mM imidazole, 20 mM taurine, 50 mM $K^{+}$-MES, 0.5 mM dithiothreitol, 6.56 mM $MgCl_2$, 5.77 mM ATP, 15 mM phosphocreatine, pH 7.1 (adjusted with KOH, at 0 °C) was prepared following Fontana-Ayoub et al 2016 (36).

Isolation medium A1: 250 mM sucrose, 0.5 mM $Na_2EDTA$, 10 mM Tris, pH 7.4, adjusted at 0 °C (36).

Isolation medium B1: prepared fresh on the day of the experiment with 50 mL Isolation medium A1 and 50 mg BSA.

MiR05, mitochondrial respiration medium: prepared from MiR05-Kit (Oroboros Instruments, Austria, 60101-01) and BSA, pH 7.1 adjusted with KOH 5 M at 30 °C (37) (Table 1).

Mitochondrial respiration and calcium medium (MiRCa): pH 7.1 adjusted with KOH 5 M at 30 °C (Table 1).

**Table 1:** Composition of media MiR05 and MiRCa.

| Chemical | MiR05 | MiRCa |
|---|---|---|
| EGTA | 0.5 mM | - |
| $MgCl_2$ | 3 mM | 1 mM |
| Lactobionic acid | 60 mM | - |
| Taurine | 20 mM | - |
| $KH_2PO_4$ | 10 mM | 10 mM |
| HEPES | 20 mM | 20 mM |
| Sucrose | 110 mM | 110 mM |
| KCl | - | 70 mM |
| BSA | 1 $g \cdot L^{-1}$ | - |
| pH (30 °C) | 7.1 | 7.1 |

The other chemicals were prepared as in Komlodi et al 2021 (38). All solutions and media were aliquoted and stored at -20 °C, unless otherwise stated.

## Animals

Wild-type C57BL/6N female and male adult mice (average age 15 ± 5 weeks) were provided and housed in the animal facility of Medical University of Innsbruck at a maximum number of five animals per cage. Animals were maintained in a controlled environment (22 °C, 12/12 h light/dark cycle, light period from 7:00 to 19:00) and fed *ad libitum* with free access to water. Mice were killed by cervical dislocation, and the liver was immediately removed and placed in ice-cold BIOPS. All procedures were conducted according to the Austrian Animal Experimentation Act in compliance with the European convention for the protection of vertebrate animals used for experimental and other scientific purposes (Tierversuchsgesetz 2012; Directive 2010/63/EU; BMWFM-66.011/0128-WF/V/3b/2016).

## Mitochondrial preparation

Liver mitochondria were isolated as described (39), with modifications. All steps were performed on ice. Briefly, after determination of wet mass, the liver was

extensively washed with ice-cold BIOPS and minced with scissors in medium A1 with at least three changes of medium A1 during mincing. The tissue was transferred to a pre-cooled glass/Teflon potter and homogenized in 20 mL of medium A1 with 5 strokes at ~300 rpm (WiseStir HS-30E, Wisd Laboratory Instruments, Wertheim, Germany), followed by centrifugation at 600 *g* for 10 min at 4 °C (Rotina 380R, Andreas Hettich GmbH & Co. KG, Tuttlingen, Germany). If a fluffy white layer was present on top of the supernatant, it was removed with a pipette. The supernatant was subsequently centrifuged for 10 min at 10 000 *g* at 4 °C. The supernatant was discarded, and the pellet resuspended with a pipette in 1 mL medium B1, then homogenized with a small glass/Teflon potter in total 5 mL medium B1 with 5 strokes at ~300 rpm. 5 mL B1 were added, and the pellet was centrifuged twice at 10 000 *g* for 10 min at 4 °C and resuspended with a pipette in 10 mL medium B1 after the 3$^{rd}$ centrifugation. Finally, after the 4$^{th}$ centrifugation, the pellet was resuspended in the proportion of 1 g tissue (whole liver wet mass) per 0.5 mL medium B1. The sample was kept on ice for at least 30 min before experiments. Five µL (only respiratory experiments) or 10-20 µL ($Ca^{2+}$ experiments) of isolated mitochondria (imt) were added to the 2-mL chambers and the experimental concentration was calculated after protein determination.

Protein was determined using the kit DC Protein Assay (Bio-Rad, Hercules, CA, US), as previously described (38, 40).

**HEK 293T cells culture and cryopreservation**

HEK 293T cells (ATCC® CRL-3216™, RRID:CVCL_0063) were obtained from the American Type Culture Collection through LGC Standards (Wesel, Germany). Cells were cultured and cryopreserved in the Institute of Biochemistry, University of Innsbruck (41). After 9-21 weeks of cryopreservation at -80 °C, the vial with 250 µL of cells were thawed, resuspended in 750 µL MiRCa, diluted 1:20 in MiRCa and mixed 1:1 with trypan blue for counting with a Countess II AMQAX1000 Automated Cell Counter (Thermo Life Technologies, Carlsbad, CA, USA) as described (41). $2{\cdot}10^6$ cells with viability between 87-93 % were added to each chamber, and data were normalized by total cell concentration.

**High-resolution respirometry and calcium measurements**

$Ca^{2+}$ was measured concomitantly with oxygen consumption using the Oroboros Bioenergetics Platform and the software DatLab 7.4 or 8 (Oroboros Instruments, Innsbruck, Austria). Measurements were performed at 37 °C in closed 2-mL Durane glass chambers using black PEEK stoppers and white PVDF stirrer bars at a rotation speed of 750 rotations per minute. $O_2$ concentration was measured with calibrated polarographic oxygen sensors (POS), and volume-specific $O_2$ consumption was calculated real-time as the negative time derivative of $O_2$ concentration. The $O_2$ flux was corrected for the instrumental $O_2$ background which was assessed at monthly intervals as part of quality control along with daily air calibration (42). A polarization voltage of 800 mV was applied to the POS. The data recording interval was set at 2 seconds. Respiratory results were expressed as protein-mass specific $O_2$ flux $J_{O2}$

[pmol·s$^{-1}$·mg$^{-1}$] or cell-count specific $O_2$ flow $I_{O2}$ [amol·s$^{-1}$·x$^{-1}$]. Fluorescence was measured with Blue Smart Fluo-Sensors inserted through the front window of the chamber, at excitation wavelength 465 nm and filters for LED and photodiode selected for CaG. Light intensity in the Fluo channel of 500 and gain 1000 were the amperometric parameters applied and the raw data were recorded as current [nA]. Glutamate increased the background fluorescence signal, while malate decreased and balanced it. Taken together, no chemical correction had to be applied.

The coupling- and pathway-control protocol SUIT-008 (https://wiki.oroboros.at/index.php/SUIT-008_O2_mt_D026; retrieved 2026-07-08) was applied to compare respiration in MiR05 and MiRCa media in the presence or absence of CaG, with the same fluorescence settings as in $Ca^{2+}$ measurements. Rates were determined in the three coupling states, leak respiration *L*, OXPHOS capacity *P*, and electron transfer (ET) capacity *E*. After addition of liver imt (residual endogenous substrates *ren*), pyruvate 5 mM and malate 2 mM (PM) were added as a combination of substrates for the NADH-linked pathway ($PM_L$). This was followed by addition of ADP (D, 2.5 mM; $PM_P$), then cytochrome *c* (*c*, 10 µM; $PM(c)_P$), glutamate (G, 10 mM; $N_P$), and succinate (S, 10 mM; $NS_P$). The uncoupler CCCP was titrated in multiple steps (U; 0.5 to 3.5 µM) until maximum respiration ($NS_E$) was achieved. Then, rotenone (Rot, 0.5 µM; $S_E$), and antimycin A (Ama, 2.5 µM; *rox*) were added sequentially. All mitochondrial respiratory rates were baseline-corrected for residual oxygen consumption (*rox*), except if stated in figure legends (43).

CaG does not cross cellular membranes. Therefore, extramitochondrial $Ca^{2+}$ was measured. The SUIT-035 protocol was applied for concomitant $Ca^{2+}$ and oxygen measurements in liver imt and HEK293T permeabilized cells using MiRCa as respiration medium. Addition of CaG 2 µM was followed by glutamate (G, 10 mM) and malate (M, 2 mM) as NADH-linked substrates. In some experiments, CsA (1 µM) was added before the substrates. Then, ADP was added at a low concentration (D.03, 30 µM), which corresponds to the cytosolic concentration at cellular resting states (44, 45). This ensures $Ca^{2+}$ uptake in response to $Ca^{2+}$ titrations, while preventing mtPT in the early phase of $Ca^{2+}$ uptake (46). Oligomycin (Omy, 20 nM or 2.5 µM) was added to ensure that mtMP was not lowered by ATP production through ATP synthase. The mtMP is required for $Ca^{2+}$ uptake via MCU. EGTA 15 µM was added to chelate the $Ca^{2+}$ contamination of the medium and chemicals, followed by addition of liver imt (~0.1 mg·mL$^{-1}$), and $CaCl_2$ ($Ca^{2+}$) titrations in 5 µM steps to generate a '$Ca^{2+}$ load', unless otherwise stated in figure legends. Finally, uncoupler was titrated after mtPT to ensure that all $Ca^{2+}$ was released.

Some experiments were run with double mitochondrial protein concentrations (~0.2 mg·mL$^{-1}$). In another variation, ATP (1 mM) was added at the beginning of the assay. Preliminary tests were conducted comparing the 5 µM $Ca^{2+}$ titrations with its carrier ($H_2O$) or with 2.5 µM $Ca^{2+}$. $CaCl_2$ titration steps should be optimized based on sample concentration and tissue type, as mtPT induction thresholds vary with tissue origin and potential sensitizing factors (47).

A similar protocol was applied to measure $Ca^{2+}$ and oxygen consumption in cryopreserved HEK293T cells. Cells (ce) were permeabilized by digitonin (Dig, 10 $\mu g \cdot mL^{-1}$). The order of titrations was slightly changed to ce;CaG;CsA(optional);EGTA*;Dig;G;M;D0.03;Omy;Ca* (asterisks indicate multiple titrations).

The Titration-Injection microPump (TIP2k, Oroboros Instruments, Innsbruck, Austria) was used for some measurements. The syringes were filled with 10 mM $CaCl_2$ following the manufacturer's instructions (48). The TIP2k was programmed to titrate 0.5 or 1 µL of $CaCl_2$ (2.5 and 5 µM experimental concentration, respectively) for one second every 5 or 6 minutes. For continuous $Ca^{2+}$ injections the TIP2k was set to inject 10 nM of $Ca^{2+}$ per second (2 $nL \cdot s^{-1}$). At such a low volume-injection rate the amount of $O_2$ added into the chamber with the $CaCl_2$ solution is negligible and corrections are not required (49). The titrations were stopped manually after $Ca^{2+}$ release was observed.

In initial experiments with imt, EGTA was titrated in 5 µM steps until no further decrease was observed in the CaG signal. In subsequent experiments, a single EGTA titration of 15 µM was applied. The EGTA concentration was evaluated for every sample type and medium batch, as some chemicals used to prepare media contain low $Ca^{2+}$ concentrations, which must be chelated before titrating the sample. If the EGTA concentrations are too high, the CaG signal does not respond to $CaCl_2$ titrations. Conversely, if EGTA concentrations are too low, mitochondria take up contaminant $Ca^{2+}$ from the medium before the $Ca^{2+}$ titrations. The latter would be observed as a gradual decrease in the CaG signal after adding mitochondria, instead of the rapid decrease of the signal due to optical interference and subsequent stabilization. In the experiments with cells, EGTA was titrated stepwise before permeabilization of the cells. This is important since the cryopreservation solution contains fetal bovine serum (FBS) with high $Ca^{2+}$ concentration and can vary from batch to batch.

The concentration of sodium added in conjunction with glutamate (10 mM) was in the physiological range (50) and guarantees functional $Ca^{2+}$ homeostasis, with both $Ca^{2+}$ uptake by MCU and release by NCLX (51). Sodium in pyruvate (5 mM) and succinate (20 mM) as used in SUIT-008 increases the experimental $Na^+$ concentration.

**Calibrations of the Calcium Green signal**

The CaRC can be calculated from $Ca^{2+}$ additions required to trigger mtPT monitored by swelling, inhibition of the $O_2$ flux, or increase of the non-calibrated CaG signal (52-57). To obtain the actual $Ca^{2+}$ concentration in solution, the $Ca^{2+}$ signal must be calibrated taking into account the non-linearity of fluorescence methods (58). Without standardized calibration, reproducibility between studies is compromised.

Using a spectrofluorometer, it is possible to obtain calibrations which consider the $K_d$ (50, 59) and maximal and minimal fluorescence, applied to (Eq. 1),

$$[Ca^{2+}] = K_d \cdot \frac{(F - F_{min})}{(F_{max} - F)} \qquad \text{Eq. 1}$$

Under the present experimental conditions used to measure $Ca^{2+}$ (CaG concentration, light intensity, and gain setting), the high $Ca^{2+}$ concentration required to obtain $F_{max}$ would saturate the amplifier at a maximum of 10 µA. A lower CaG concentration, gain setting, and light intensity avoid this limitation but compromise the sensitivity of $Ca^{2+}$ measurements.

Another possibility is to obtain $Ca^{2+}$ calibration curves with $Ca^{2+}$ titrations (60). Such calibration curves were obtained under experimental conditions, in the absence or presence of mitochondria with inhibited $Ca^{2+}$ uptake. We used the MCU inhibitor ruthenium red (RR, 1 µM) and encountered the disadvantage of carry-over of an inhibitory effect to subsequent experiments even after rigorous cleaning of the experimental chambers. Alternatively, an inhibitor cocktail containing rotenone and antimycin A, and the uncoupler CCCP (Rot, 0.5 µM; Ama, 2.5 µM; and CCCP, 1 µM) was used to inhibit the mitochondrial electron transfer system, collapsing the protonmotive force. The TIP2k was programmed to inject 1 µL of $CaCl_2$ in one second every 2 minutes, to a total of 10 titrations of 5 µM $CaCl_2$ each. To calculate the extramitochondrial $Ca^{2+}$ concentration, the CaG raw fluorescence signal ($I$, nA) obtained during sections (defined as marks in DatLab) after each $CaCl_2$ titration with known concentration were fitted by a second-degree polynomial (Eq. 2). Detailed results are presented in supporting information A (Figures S1-S3).

$$[Ca^{2+}] = aI^2 + bI + c \qquad \text{Eq. 2}$$

In the $Ca^{2+}$ uptake experiments performed with several $Ca^{2+}$ titrations (Figure 3), marks were set for each 5 µM $Ca^{2+}$ titration at the highest CaG signal and subsequently at the lowest signal diminished due to $Ca^{2+}$ uptake. After the experiment, with the same sample, the above calibration was performed and the fluorescence raw values (nA) of the marks from the $Ca^{2+}$ uptake experiments were applied for polynomial fitting.

Figure S4 shows the calculated concentration differences $\Delta Ca^{2+}$ in response to $Ca^{2+}$ titrations. Unexpectedly, from the third titration onwards, the majority of calculated $\Delta Ca^{2+}$ concentrations were higher than the 5 µM step. Theoretically, however, only lower values than the 5 µM steps might be expected due to rapid $Ca^{2+}$ uptake or chelation by medium components. The fluorescence signals before the first $Ca^{2+}$ titration were similar in experiments with functional mitochondria and calibrations with inhibited mitochondria and cannot explain the observed differences. We currently lack a mechanistic explanation for the apparent >5 µM $Ca^{2+}$ concentration response. In conclusion, the polynomial calibration method is unreliable under these experimental conditions. Therefore, we developed an intra-experimental calibration approach.

**Intra-experimental calibration**

To convert changes in fluorescence to changes in $Ca^{2+}$ concentration, the sequential 5 µM $Ca^{2+}$ titrations, $\Delta c_{in(i)}$ (Figure 1a), were divided by the corresponding step changes in fluorescence signal $\Delta FS_i$, where $i$ indicates sequential titrations, $\Delta FS_{ui}$ is the decrease in the fluorescence signal during uptake phase $i$, and $\Delta FS_i$ is (Figure 1b),

$$\Delta FS_i = FS_i - FS_{u(i-1)} \quad [\mu A] \quad \text{Eq. 3}$$

The corresponding calibration factor $f_i$ is (Eq. 4),

$$f_i = \frac{\Delta c_{in(i)}}{\Delta FS_i} \quad [\mu M/\mu A] \quad \text{Eq. 4}$$

Table 2 summarizes the definitions of abbreviations used in the calibration equations. $\Delta FS_i$ and hence $f_i$ changed as a nonlinear function of the titration steps $i$ (Figure 1c to e). Therefore, the following equation was used to calculate average calibration factors $f_{calc(i)}$,

$$f_{calc(i)} = \frac{\Delta c_{in(i)}}{\Delta FS_{calc(i)}} \quad [\mu M/\mu A] \quad \text{Eq. 5}$$

where $\Delta FS_{calc(i)}$ is

for $r_{ui} < 1$ $$\Delta FS_{calc(i)} = \frac{(1+r_{ui})\cdot\Delta FS_i + (1-r_{ui})\cdot\Delta FS_{i+1}}{2} \quad [\mu A] \quad \text{Eq. 6a}$$

for $r_{ui} > 1$ $$\Delta FS_{calc(i)} = \frac{(1+r_{ui})\cdot\Delta FS_{i-1} + (1-r_{ui})\cdot\Delta FS_i}{2} \quad [\mu A] \quad \text{Eq. 6b}$$

During titration interval $i$, the fluorescence signal declines due to $Ca^{2+}$ uptake by $\Delta FS_{ui}$ (see Figure 1b),

$$\Delta FS_{ui} = FS_i - FS_{ui} \quad [\mu A] \quad \text{Eq. 7}$$

The $Ca^{2+}$ uptake ratio $r_{ui}$ is

$$r_{ui} = \frac{\Delta FS_{ui}}{\Delta FS_i} \quad \text{Eq. 8}$$

When $r_{ui} < 1$, the uptake was incomplete and $\Delta FS_{calc(i)}$ was calculated from $\Delta FS_i$ and $\Delta FS_{i+1}$, the step changes in fluorescence before and after the $Ca^{2+}$ uptake (Figure 1b, $i = 3$). When $r_{ui} > 1$, the uptake was higher than $\Delta c_{in(i)}$, and $\Delta FS_{calc(i)}$ was calculated from $\Delta FS_{i-1}$ and $\Delta FS_i$ by interpolation (Figure 1b, $i = 4$).

$Ca^{2+}$ uptake $\Delta c_{ui}$ was calculated as the decrease in the fluorometric signal $\Delta FS_{ui}$ multiplied by the calibration factor $f_{calc(i)}$,

$$\Delta c_{ui} = f_{calc(i)} \cdot \Delta FS_{ui} \quad [\mu M] \quad \text{Eq. 9}$$

$n$ is the titration step $i$ after which the fluorescence signal increased due to mtPT. The apparent calcium uptake capacity (CaUC', not normalized for mitochondrial protein; Figure 1b) is calculated as,

$$CaUC' = \sum_{i=1}^{n} \Delta c_{ui} \quad [\mu M] \quad \text{Eq. 10}$$

After the $n^{th}$ titration, $Ca^{2+}$ uptake $\Delta c_{un}$ is calculated up to the minimum fluorescence signal monitored before signal inversion indicating $Ca^{2+}$ release (Figure 1b; $n = 6$).

**Table 2: Abbreviations from Equations 3-10 and Figure 1.**

| Abbreviation | Definition | Eq. |
|---|---|---|
| $i$ | sequential $Ca^{2+}$ titration, single step | |
| $FS_i$ | peak of fluorescence signal after titration $i$ | (3) |
| $FS_{ui}$ | fluorescence signal at the end of uptake period $i$ | (3) |
| $\Delta FS_i$ | step change in fluorescence signal in titration $i$ | (3) |
| $f_i$ | calibration factor $i$ | (4) |
| $\Delta c_{in(i)}$ | change of $Ca^{2+}$ concentration due to titration $i$ | (4, 5) |
| $f_{calc(i)}$ | average calibration factor $i$ | (5) |
| $\Delta FS_{calc(i)}$ | step change in fluorescence signal calculated | (6) |
| $\Delta FS_{i+1}$ | step change in fluorescence signal in titration $i$+1 | (6a) |
| $\Delta FS_{i-1}$ | step change in fluorescence signal in titration $i$-1 | (6b) |
| $\Delta FS_{ui}$ | decrease in the fluorescence signal during uptake phase $i$ | (7) |
| $r_{ui}$ | $Ca^{2+}$ uptake ratio | (8) |
| $\Delta c_{ui}$ | change of concentration due to $Ca^{2+}$ uptake | (9) |
| $n$ | number of titration steps after which mtPT occurs | (10) |
| CaUC‘ | apparent $Ca^{2+}$ uptake capacity | (10) |

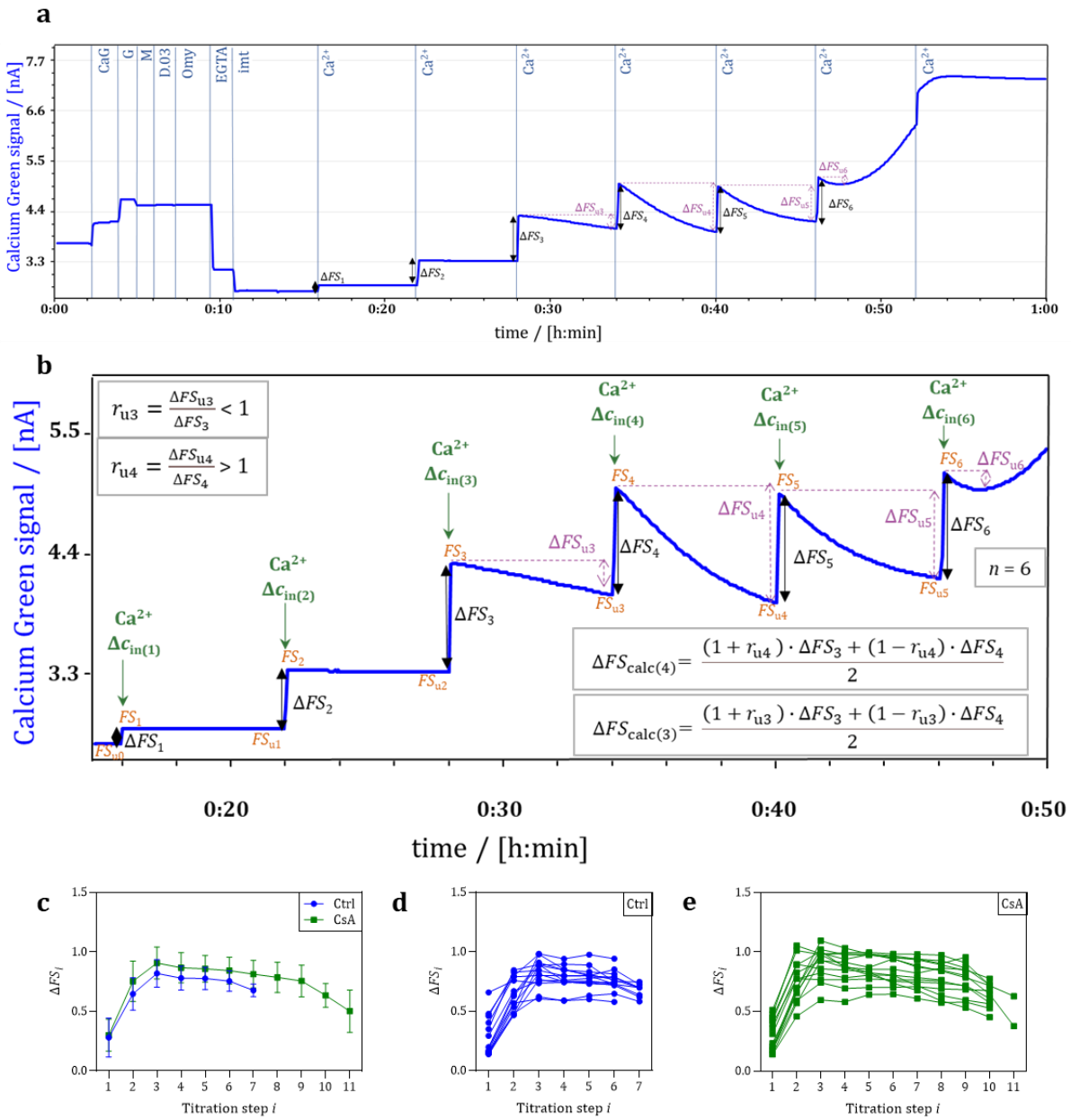


**Figure 1. Intra-experimental calibration of calcium signal.** $\Delta FS_i$ is the difference of the peak fluorescence signal *FS* measured after a 5 µM $Ca^{2+}$ pulse ($\Delta c_{in}$) and the fluorescence signal *FS* immediately before the titration. $\Delta FS_{ui}$ is the difference between the peak $FS_i$ and the *FS* immediately before the next $Ca^{2+}$ titration. **(a)** Representative trace indicating $\Delta FS_i$ and $\Delta FS_{ui}$ used in Eq. 3-8. Black arrows indicate $\Delta FS_i$ and purple dashed arrows indicate $\Delta FS_{ui}$. All $\Delta FS_{ui}$ were summed to provide corrected CaUC. Experiment 2021-09-02 P3-02. **(b)** Zoom from panel (a). Green arrows represent 5 µM $Ca^{2+}$ titrations, $\Delta c_{in}$. The $\Delta FS_{calc(i)}$ equation (as shown) changes if uptake was higher than the respective $\Delta FS_i$ ($r_{ui}$>1) or if the uptake was incomplete ($r_{ui}$<1). **(c), (d)** and **(e)** show $\Delta FS$ for each $Ca^{2+}$ titration step *i* from all experiments. Blue lines represent experiments in absence of CsA (Ctrl) and green lines in the presence of CsA. Mean ± SD in **(c)** and each replicate in **(d)** and **(e)**. See Table 2 for definition of abbreviations. Protocol: CaG (2 µM); G (10 mM); M (2 mM); ADP (30 µM); Omy (2.5 µM); EGTA (15 µM); imt; $Ca^{2+}$ (5 µM each).

Data analysis of $O_2$ measurements in SUIT-008 was performed using Excel templates provided with DatLab and statistical analyses of all experiments were performed with GraphPad Prism version 9 or 10.

## 3. Results

**Effect of medium and the fluorophore CaG on respiration**

Formulating a medium that suits both $Ca^{2+}$ uptake analysis and respiration was a challenge. The most suited medium for respiration, MiR05, cannot be used to analyze $Ca^{2+}$ uptake due to several components that interfere with the $Ca^{2+}$ signal, such as high concentration of EGTA, lactobionic acid, taurine, and BSA (28). On the other hand, media used for $Ca^{2+}$ uptake measurements frequently contain low phosphate concentration and high KCl concentration, which decrease respiratory rates (61, 62). Mitochondrial Respiration and Calcium Medium MiRCa, containing a low KCl concentration and the same phosphate concentration as MiR05 was developed to measure simultaneously respiration and CaG. MiRCa and MiR05 had identical mass-specific mitochondrial $O_2$ flux (*rox* corrected) supported by pyruvate, malate, and glutamate (N-pathway), plus succinate (NS-pathway) in different coupling states, and the S-pathway after inhibition by rotenone (Figure 2, *p*-values comparing media effects in supporting information B Table S1).

There was no effect of CaG on mitochondrial $O_2$ flux (Figure 2a; $p > 0.3$), as highlighted by expressing respiration in the presence of CaG relative to controls (Figure 2b). Flux control ratios (*FCR*) are statistically more robust to evaluate differences in mitochondrial respiratory control patterns. *FCR* were not different in MiRCa and MiR05 (Figure 2c), except for a possible trend of MiRCa for a lower $S_E/NS_E$ ratio (6Rot in Table S2), and $N_P/NS_E$ in the presence of CaG (2D and 2c in Table S2; comparison of the presence versus the absence of CaG in *FCR* generated $p > 0.3$). When combining groups with and without CaG, lower *p*-values were observed in $NS_P$ and $S_E$ in both protein mass-specific $O_2$ flux and *FCR* (Tables S3 and S4). Figure 2d shows the relative media effect. These results indicate that comparable to MgG, CaG does not affect respiration, and MiRCa is a suitable medium for combined respiration and calcium measurements using CaG.

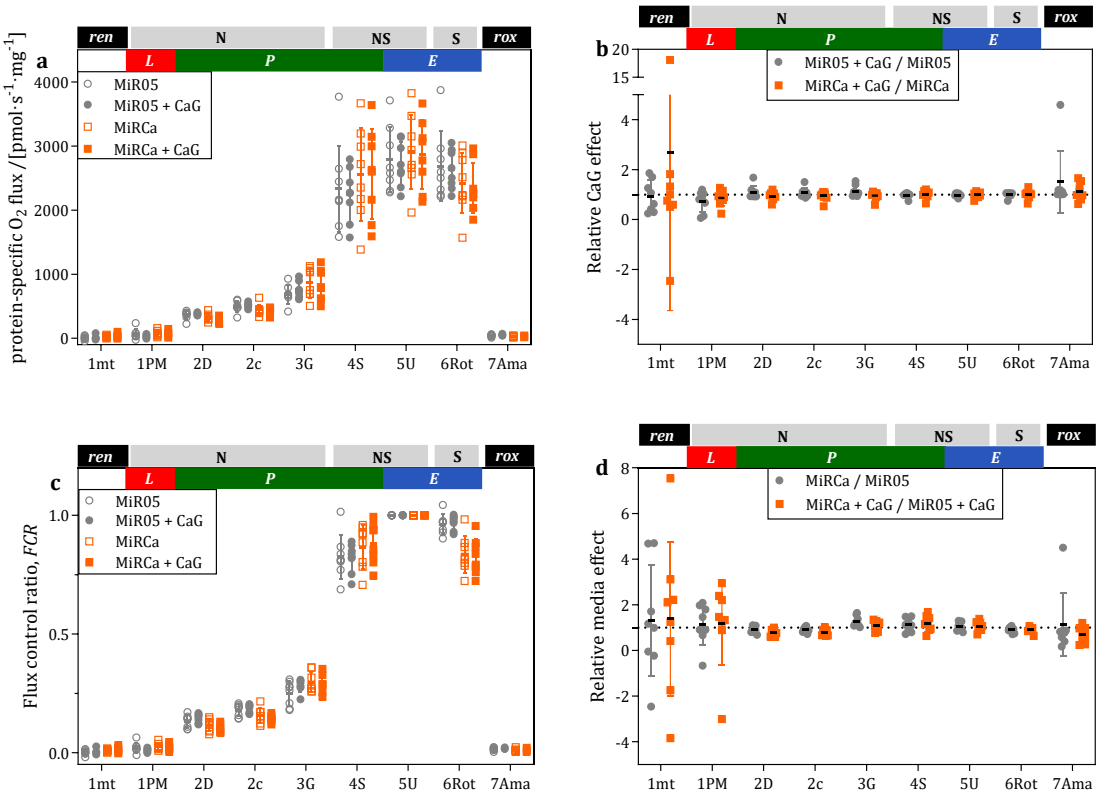


**Figure 2. The effect of MiR05 versus MiRCa media and CaG on $O_2$ consumption of mitochondria isolated from mouse liver.** HRR with coupling control protocol SUIT-008_O2_mt_D026, before addition of substrates (*ren*), N-, NS-, and S-linked pathways in different coupling states, and finally *rox* after inhibition by Ama. The sequential titrations are indicated on the abscissas. Different symbols and colors indicate the treatments, each symbol represents an independent mitochondrial preparation, and for every preparation, all treatments were tested in parallel at the same time. **(a)** Mitochondrial protein-specific flux, *rox*-corrected, except for 7Ama. **(b)** Relative CaG effect calculated as the ratio of $O_2$ fluxes measured with and without CaG. **(c)** *FCR* *rox*-corrected, except for 7Ama. **(d)** Relative media effect calculated by dividing $O_2$ fluxes measured with MiRCa by those measured with MiR05, in the presence or absence of CaG. Means ± standard deviation, SD. Sample protein concentration 0.0554 ± 0.0068 mg·mL$^{-1}$ (mean ± SD). *N* = 8.

## Calcium uptake

Representative traces show simultaneously monitored mitochondrial respiration (Figure 3a) and the CaG signal in a sequence of $Ca^{2+}$ titrations (Figure 3b). Glutamate & malate were used as substrates in the leak state. Since CaG is membrane impermeable, the fluorescence signal is a function of the $Ca^{2+}$ concentration in the incubation medium outside the mitochondria. The present protocol with glutamate and malate as substrates is used as an example. There might be differences in the calcium uptake capacity (10, 63) and on the effect on respiration depending on the substrates used (50).

$O_2$ flux increased transiently during episodes of $Ca^{2+}$ uptake after 5 µM $Ca^{2+}$ titrations and returned to pre-titration levels when the rate of $Ca^{2+}$ uptake levelled off (Figure 3a). The respiratory response to 2.5 µM titrations was too low to be resolved from noise (Figure S5a) and it was similar to the response to the continuous $Ca^{2+}$ injection (Figure S6a). mtPT led to a sharp inhibition of respiration to a constant level. Uncoupler titration (CCCP, 1 µM) at this inhibited state did not stimulate respiration, providing evidence for the irreversible destruction of mitochondrial respiratory control induced by mtPT.

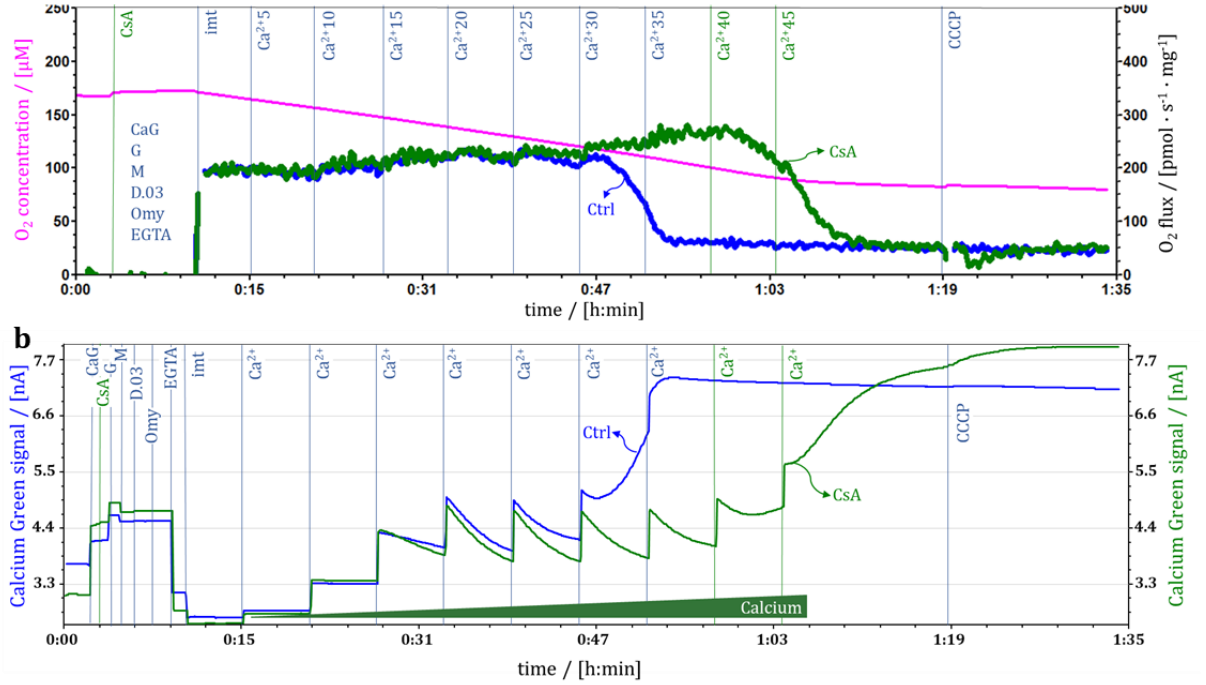


**Figure 3: Simultaneous measurement of (a) respiration and (b) calcium uptake by high-resolution respirometry with the Oroboros Fluo Smart-Module in mitochondria isolated from mouse liver.** Representative traces of the calcium uptake protocol (SUIT-035_CaG_D083) with glutamate (G, 10 mM) and malate (M, 2 mM) as substrates in the leak(Omy) state. Cyclosporin A (CsA, 1 µM), Calcium Green (CaG, 2 µM), substrates, ADP (30 µM), Oligomycin (Omy, 2.5 µM), and EGTA (15 µM) were added before isolated mitochondria (imt). Subsequently, $CaCl_2$ was titrated in 5 µM steps ($Ca^{2+}$) every 6 min until calcium release was observed as a sudden increase in the CaG signal. Dark blue vertical lines represent events in both chambers, green in the chamber with CsA. (a) $O_2$ concentration (pink line), specific $O_2$ flux in the absence (blue line, Ctrl) or presence of CsA (green line, CsA). (b) CaG signal in the absence (blue line, Ctrl) or presence of CsA (green line, CsA). Experiment 2021-09-02 P3-02.

Titration of $H_2O$ ($Ca^{2+}$ carrier) did not cause transient increases of $O_2$ flux (Figure S7a), confirming that the effect of $Ca^{2+}$ titrations was distinct from noise. These transient increases are related to $Ca^{2+}$ uptake (Figure S7b) driven by the protonmotive force which causes an increase of respiration above the $O_2$ consumption in the leak state. During $Ca^{2+}$ uptake, $O_2$ consumption cannot be considered as idle leak

respiration, since net $Ca^{2+}$ uptake against a concentration difference represents biochemical work.

Figure 3a and S8 represent the most commonly observed pattern of respiration which, in the presence of CsA, increased with additional $Ca^{2+}$ titrations beyond those triggering mtPT in controls. In one mitochondrial preparation (four technical repeats) no corresponding increase in leak respiration was observed (Figure S9). In another preparation, one of two technical repeats showed an irregular pattern of leak respiration in both Ctrl and CsA (Figure S10).

The response of the $Ca^{2+}$ signal was small and no $Ca^{2+}$ uptake was detected after the first or even second $Ca^{2+}$ titration of 5 µM (Figure 3b and S5d) or 2.5 µM (Figure S5b), most probably due to binding by the initially added EGTA (15 µM) (51). A lower response of the $Ca^{2+}$ signal indicates EGTA chelation upon the initial titration steps, while a constant increase during later titrations indicates that EGTA chelation was saturated. There was no $Ca^{2+}$ uptake, up to a total addition of 10 µM, even if the signal was responsive to $Ca^{2+}$ titrations. This reflects the high apparent $K_d$ of the MCU, requiring elevated $Ca^{2+}$ levels to trigger mitochondrial $Ca^{2+}$ uptake (5). Upon two or more additional $Ca^{2+}$ titrations, $Ca^{2+}$ uptake was complete in each step, as indicated by the decline of the $Ca^{2+}$ signal to the level obtained before the titration (Figure 3b). An increase of the $Ca^{2+}$ signal beyond the titrated concentration indicated mtPT. Towards mtPT, $Ca^{2+}$ uptake was incomplete, i.e., less than the 5 or 2.5 µM titrated. CsA delayed mtPT (Figure 3b, green line), and in its presence the uncoupler titration accelerated calcium release, but not in its absence. Figure S5 compares 2.5 and 5 µM $Ca^{2+}$ titrations and Figure S7b compares the CaG signal in $Ca^{2+}$ and carrier titrations.

In preliminary tests, in controls with 2.5 µM $Ca^{2+}$ titrations the mtPT was triggered after a load of 26.6 ± 1.2 µM, corresponding to the mitochondrial protein-specific load of 280.5 ± 57.2 nmol·mg$^{-1}$ (this and all subsequent results are presented as mean ± standard deviation, SD, $N$ = 3) (Figure S5b). In contrast, when adding $Ca^{2+}$ in 5 µM steps, the mtPT was triggered at 31.6 ± 2.4 µM or 394.2 ± 171.4 nmol·mg$^{-1}$ (Figure S5d). These results support the hypothesis that lower $Ca^{2+}$ concentration steps underestimate the $Ca^{2+}$ retention capacity, probably due to the time of exposure of mitochondria to $Ca^{2+}$ (64). Conversely, larger $Ca^{2+}$ pulses may exceed physiological concentrations, such as those seen in ER/SR $Ca^{2+}$ release waves (65,66).

Figure S6 shows representative traces of mitochondrial respiration and CaG signal upon continuous injection of $Ca^{2+}$ with the TIP2k at 10 nM/s, with the same substrates mentioned previously. After the first ~2 minutes of the injection, there was barely any increase in CaG signal, due to EGTA chelation and dye binding kinetics. The cumulative injection up to this point was 1.27 ± 0.13 µM or 13.34 ± 1.51 nmol·mg$^{-1}$ (Ctrl) and 0.97 ± 0.21 µM or 10.17 ± 3.79 nmol·mg$^{-1}$ (CsA), as indicated by the first arrow in Figure S6b. Following this initial phase of slight increase, when EGTA chelation became saturated, the CaG signal exhibited a more pronounced rise until a concentration sufficient for kinetic control of the low-affinity MCU was reached (12.3 ± 1.4 µM or 129.16 ± 30.73 nmol·mg$^{-1}$ in Ctrl and 10.3 ± 0.8 µM or 108.27 ± 29.43

nmol·mg$^{-1}$ in CsA). A near steady-state was achieved where the net-uptake rate overcompensates slightly the $Ca^{2+}$ injection rate. At the point where the CaG signal increased steeply, indicating mtPT, the cumulative injected $Ca^{2+}$ was 23.45 ± 0.49 µM or 246.95 ± 39.24 nmol·mg$^{-1}$ (Ctrl) and 34.64 ± 1.78 µM or 364.75 ± 46.20 nmol·mg$^{-1}$ (CsA). The oxygen flux in response to continuous injections was similar to that in experiments with 2.5 µM $Ca^{2+}$ step titrations.

The different approaches of $Ca^{2+}$ load (single bolus, pulses with different concentrations or continuous injections) lead to different $Ca^{2+}$ supplements necessary to trigger mtPT, as observed previously (67). In that study the authors observed that the capacity of rat liver mitochondria to accumulate $Ca^{2+}$ before mtPT was 800 nmol·mg$^{-1}$ using a steady infusion, compared to 650 nmol·mg$^{-1}$ using pulses, or 450 nmol·mg$^{-1}$ in a single bolus.

**Calcium uptake capacity and calcium retention capacity**

Calcium uptake capacity (CaUC), calculated according to the intra-experimental calibration method described in this study, and calcium retention capacity (CaRC), the cumulative $Ca^{2+}$ concentration added, are compared in Figure 4a. CsA increased both CaRC and CaUC by approximately two-fold. The relation between CaRC and CaUC is shown in Figure 4b. CaUC was as low as 45 % of CaRC in controls and 55 % in the presence of CsA (Figure 4c). Both indices were normalized by mitochondrial protein mass.

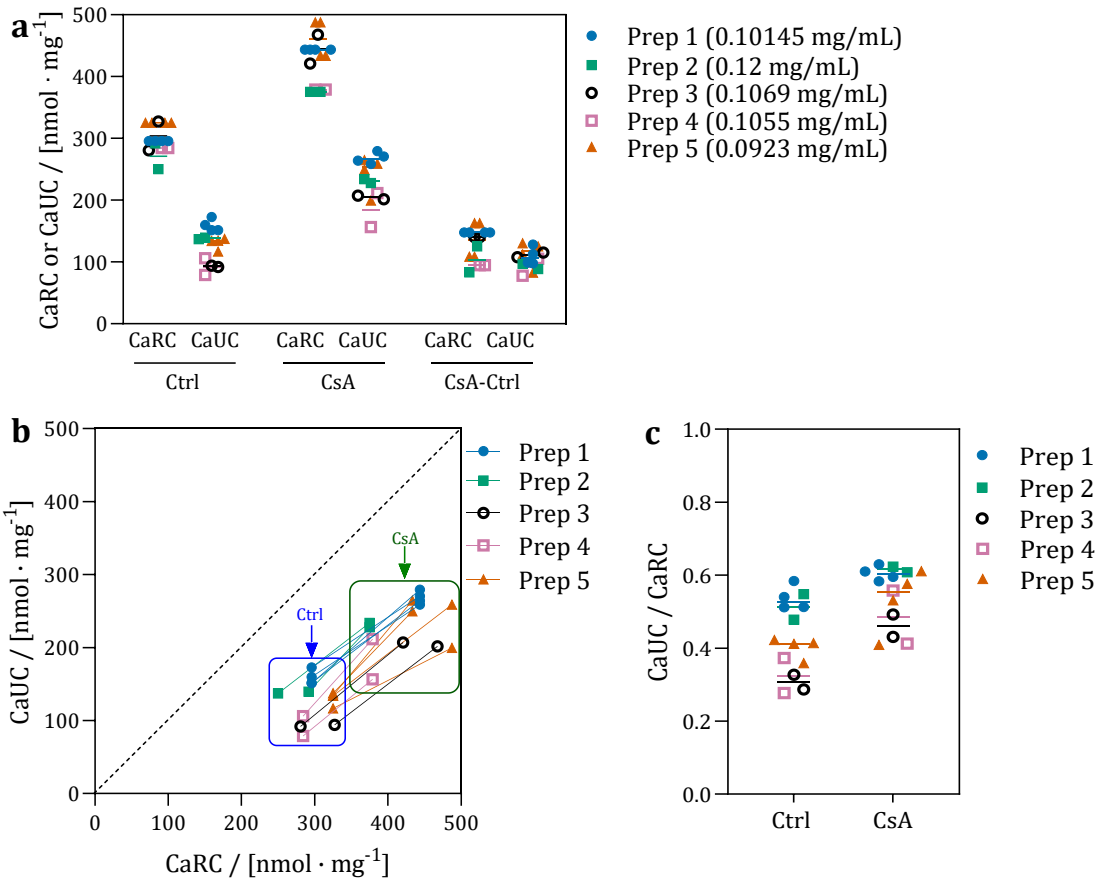


**Figure 4: Calcium retention capacity CaRC and calcium uptake capacity CaUC in isolated mitochondria. (a)** CaRC is the sum of $Ca^{2+}$ titrated until mtPT, whereas CaUC is the sum of $Ca^{2+}$ actually taken up before mtPT. Data were normalized by mitochondrial protein mass, indicated for each preparation, 0.1052 ± 0.009 mg·mL$^{-1}$ (mean ± SD). Measurements in the absence (controls, Ctrl) or presence of Cyclosporin A (CsA); CsA–Ctrl represents the difference between both measurements. Experiments were performed with 5 independent mitochondrial preparations (different symbols and colors) in two or four technical repeats (same symbol and color). Lines represent the medians for each preparation. Means ± SD and *p*-values are summarized in Table S5. **(b)** Relation between CaRC and CaUC. Lines connect experimental repeats with the same sample. **(c)** Ratio CaUC/CaRC. $p$ = 0.002 (Ctrl vs. CsA; paired Student's $t$ test) comparing the means of each preparation (Grand mean ± SD): CaUC/CaRC(Ctrl) = 0.4168 ± 0.1054; CaUC/CaRC(CsA) = 0.5397 ± 0.0692. Protocol: CaG (2 µM); G (10 mM); M (2 mM); ADP (30 µM); Omy (2.5 µM); EGTA (15 µM); imt; $Ca^{2+}$ (5 µM pulses). $N$ = 5; $n$ = 2-4.

The CaUC/CaRC ratio (Figure 4c) differed between Ctrl and CsA ($p$ = 0.002). Therefore, cumulative $Ca^{2+}$ uptake was compared for both conditions up to the $Ca^{2+}$ load preceding mtPT in the control group (cumulative $Ca^{2+}$ titrations up to 25 or 30 µM). Mitochondria exposed to CsA exhibited higher cumulative $Ca^{2+}$ uptake already before

the onset of mtPT in controls (Figure 5a), indicating that CsA not only extends the total capacity for $Ca^{2+}$ uptake but also increases the cumulative $Ca^{2+}$ uptake in the early phase of $Ca^{2+}$ loading. In a further evaluation of $Ca^{2+}$ uptake after each titration (Figure 5b), the controls were taking up less $Ca^{2+}$ from a $Ca^{2+}$ load of 25 µM onwards, although mtPT only occurred at 30 or 35 µM. There was no difference in $Ca^{2+}$ uptake up to the critical $Ca^{2+}$ load of 20 µM between the two groups ($p$ = 0.3251; paired Student's $t$ test) comparing the means of each preparation (Ctrl 74.9 ± 24.9 nmol·mg$^{-1}$; mean ± SD vs CsA 79.2 ± 23.4 nmol·mg$^{-1}$). At the critical $Ca^{2+}$ load of 20 µM onwards, $Ca^{2+}$ uptake steeply declined in controls, while with CsA there was a delayed decline towards mtPT.

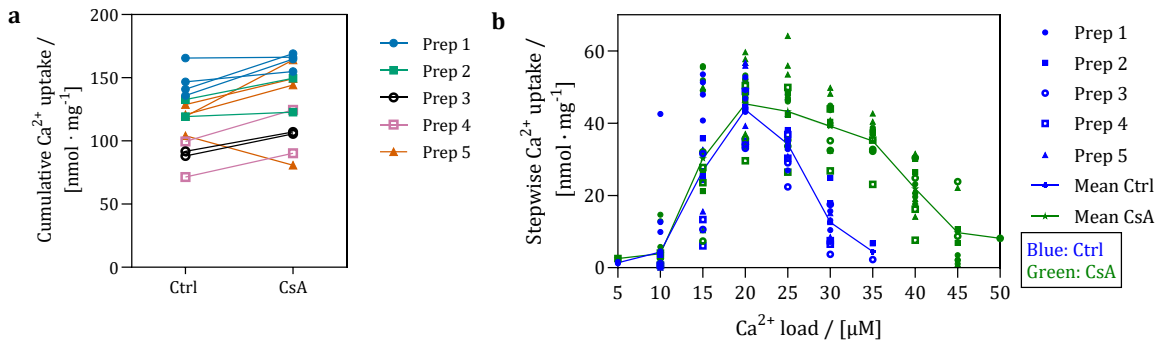


**Figure 5. Effect of Cyclosporin A (CsA) on $Ca^{2+}$ uptake normalized for mitochondrial protein mass. (a)** Cumulative $Ca^{2+}$ uptake at the $Ca^{2+}$ load (25 or 30 µM added) before controls (Ctrl) reach mtPT. $p$ = 0.0009 (paired Student's $t$ test) comparing the means of each preparation (Ctrl 113.4 ± 25.9 nmol·mg$^{-1}$; mean ± SD vs CsA 129.7 ± 23.8 nmol·mg$^{-1}$). **(b)** Stepwise $Ca^{2+}$ uptake of Ctrl (blue symbols) and CsA (green symbols) after each $Ca^{2+}$ titration representing the $Ca^{2+}$ load (different symbols for each sample preparation, and mean lines).

Since many studies with isolated mitochondria use higher sample concentrations compared to the present study, we investigated the relation between sample concentration and CaRC or CaUC. Without normalizing the data, the apparent capacities (CaRC' and CaUC'; expressed in terms of $Ca^{2+}$ concentration [µM]) were linearly dependent on mitochondrial protein concentration (Figure 6a and 6c). This highlights the importance of normalization to mitochondrial protein. Whereas CaUC [nmol·mg$^{-1}$] was independent of protein concentration (Figure 6b), CaRC [nmol·mg$^{-1}$] was negatively correlated with protein concentration (Figure 6d). The difference CaRC–CaUC follows a hyperbolic function because the effect of changes in $Ca^{2+}$ in the medium decreases as protein concentration increases (Figure 6e). When the sample concentration is extrapolated to zero, the difference tends towards infinity. A linear relationship is obtained by plotting (CaRC-CaUC)$^{-1}$ as a function of protein concentration (Figure 6f).

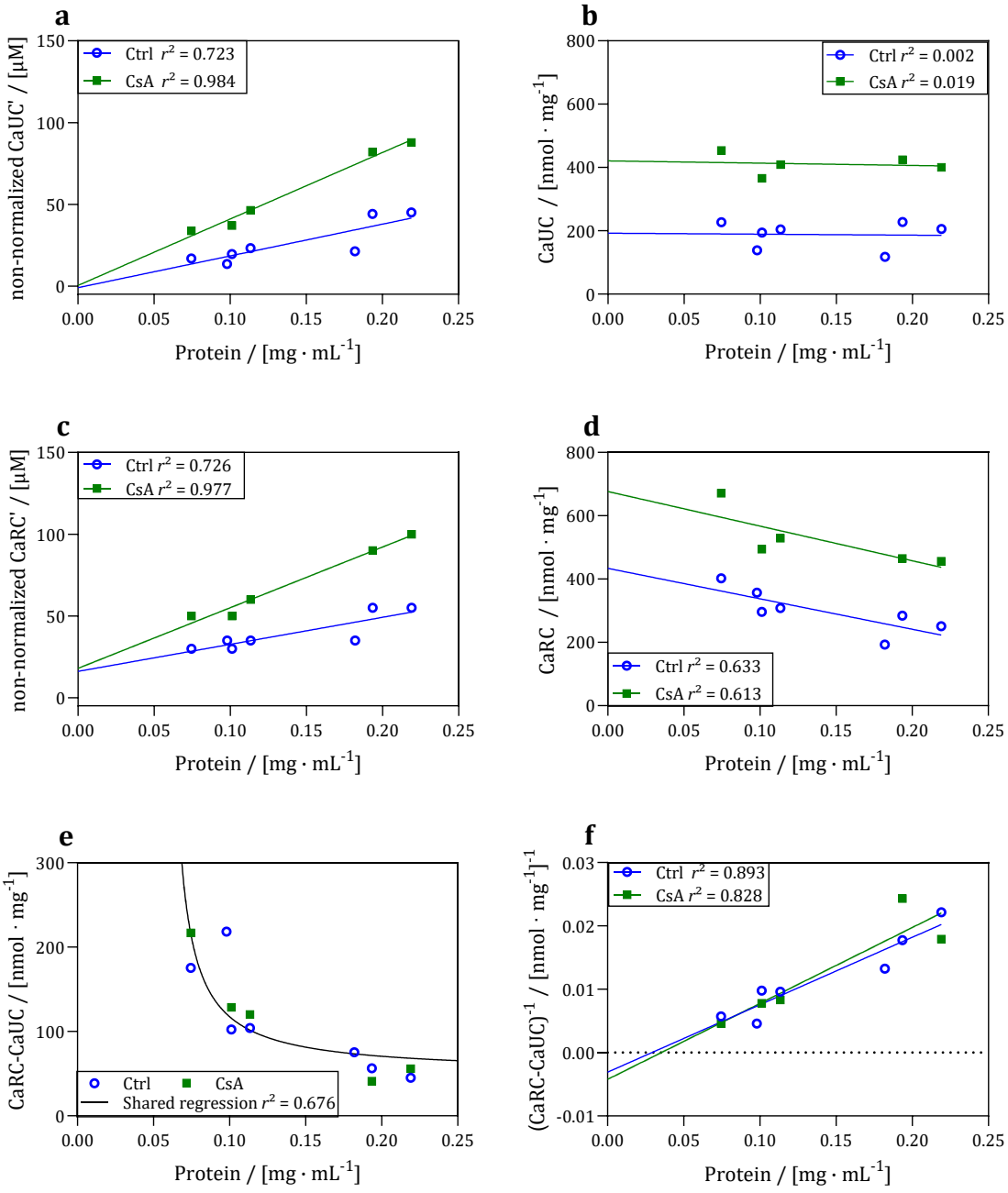


**Figure 6. Calcium uptake capacity and calcium retention capacity as a function of protein concentration in mouse liver mitochondria.** Sample concentrations ranging from 0.074 to 0.219 mg·mL$^{-1}$ were added to the chambers in the absence (Ctrl, blue open circles) or presence (CsA, green closed squares) of Cyclosporin A. (a) apparent CaUC' [µM]. (b) CaUC normalized by mitochondrial protein [nmol·mg$^{-1}$]. (c) apparent CaRC' [µM]. (d) CaRC normalized by mitochondrial protein [nmol·mg$^{-1}$]. (e) CaRC-CaUC applied to a hyperbolic fit. (f) (CaRC-CaUC)$^{-1}$ applied to a linear regression. Protocol: CaG (2 µM); G (10 mM); M (2 mM); ADP (30 µM); Omy (20 nM); EGTA (15 µM); imt; $Ca^{2+}$ (5 µM each). $r^2$ values are shown. *N* = 2-4.

Since the conditions to measure $Ca^{2+}$ uptake are sometimes criticized as non-physiological (47), we evaluated if a more physiological environment, including the presence of 1 mM ATP would change the CaUC in isolated mouse liver mitochondria (protein concentration: 0.059 $mg \cdot mL^{-1}$). In the presence of ATP, no $Ca^{2+}$ release was observed at cumulative $Ca^{2+}$ titrations up to 90 µM (green lines Figure S11). As expected, the parallel experiment without ATP (blue line) presented $Ca^{2+}$ release after cumulative titrations of 35 µM. The $Ca^{2+}$ uptake rate at which $Ca^{2+}$ is removed from the medium by mitochondria after the first $Ca^{2+}$ titration (68) was decreased in the presence of ATP compared to the group without ATP (Figure S8).

To validate the results obtained with isolated mitochondria, we performed experiments on HEK 293T cells permeabilized with digitonin. For this experiment the order of titrations was altered to add EGTA before cell permeabilization. Compared to the experiments with isolated mitochondria, a higher EGTA concentration was required to chelate $Ca^{2+}$ in the experiments with cryopreserved HEK 293T cells. Although the cryopreservation medium containing FBS was diluted before adding the cell suspension to the Oroboros chamber, the contaminant [$Ca^{2+}$] was higher in cells than in isolated mitochondria (see Methods). Overall, calcium uptake showed the same pattern as in imt, in controls or CsA (Figure 7a). CaUC compared to CaRC was 33 % lower in controls ($p$ <0.0001) and 46 % in CsA group ($p$ <0.0001; Figure 7b). The $Ca^{2+}$ concentration needed to initiate $Ca^{2+}$ uptake was higher compared to the results obtained with imt. The difference in CaRC between control and CsA was small, probably due to the high number of $Ca^{2+}$ titrations without uptake in the beginning of the $Ca^{2+}$ load ($p$ = 0.0361). The CsA effect was higher on CaUC ($p$ = 0.0072; two-way repeated measurements ANOVA, uncorrected Fisher's LSD posttest).

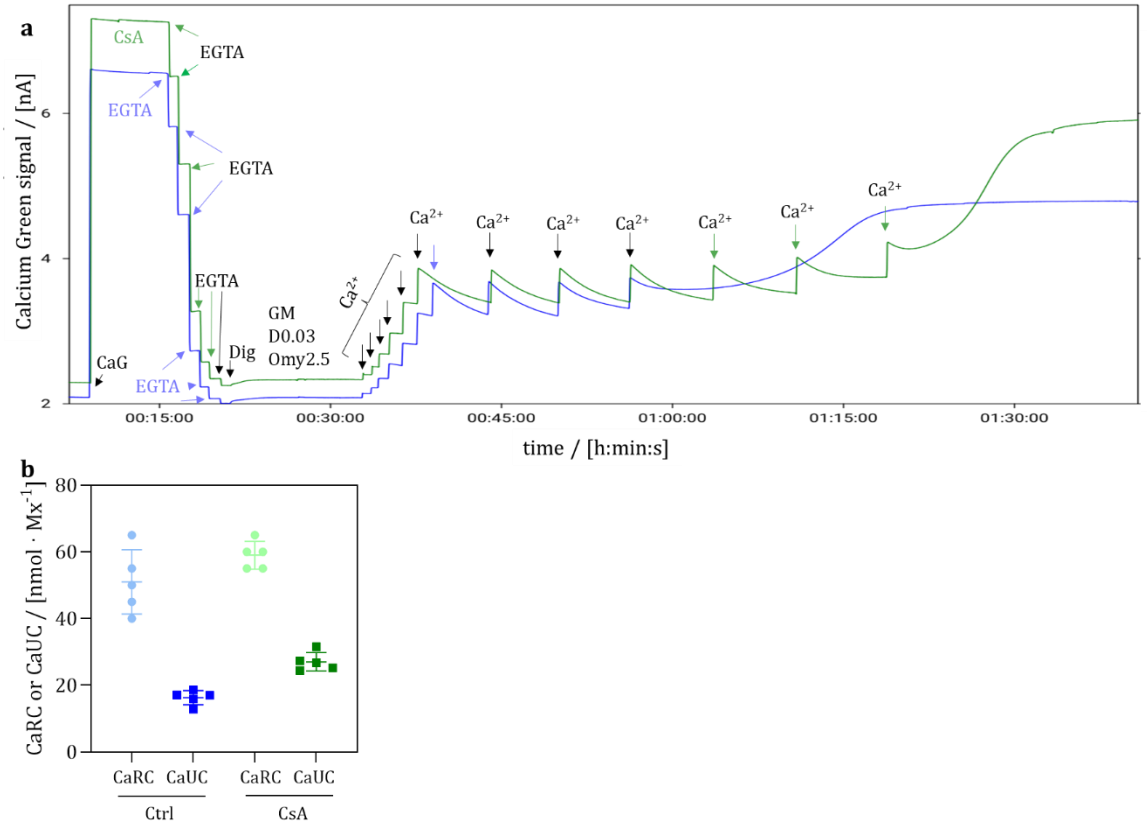


**Figure 7. Calcium retention capacity CaRC and uptake capacity CaUC in permeabilized HEK293T cells. (a)** Representative trace of the calcium uptake protocol. 1 million cells per milliliter [Mx·mL$^{-1}$] were added to the chamber before Calcium Green (CaG, 2 µM) and were permeabilized with digitonin (Dig, 10 µg·mL$^{-1}$) after EGTA titrations. Cyclosporin A (CsA, 1 µM) was added at the beginning of the assay in one chamber (green lines), while the control (blue line) was run without CsA. Glutamate (G, 10 mM) and malate (M, 2 mM) were added as substrates in the leak(Omy) state, followed by ADP (30 µM) and Oligomycin (Omy, 2.5 µM). Subsequently, $CaCl_2$ was titrated in 5 µM steps ($Ca^{2+}$) until calcium release was observed as a sudden increase in the CaG signal. The arrows (blue for control, green for CsA and black for both chambers) indicate EGTA titrations (3 of 20 µM plus 3 of 10 µM) or $Ca^{2+}$ titrations (5 µM each). File: 2022-06-21_XA-002_04 performed in DatLab 8. **(b)** CaRC and CaUC normalized by cell count. Experiments were performed with 5 independent cell vials and individual values are represented with mean ± SD.

## 4. Discussion

Calcium retention capacity (CaRC) is a term widely used in the literature and is conventionally defined as the cumulative $Ca^{2+}$ concentration (total number of $Ca^{2+}$ titrations multiplied by the concentration added in each single titration) until mitochondrial permeability transition (mtPT) occurs (25, 31, 54, 69-71). Measurement of $Ca^{2+}$ concentration in the mitochondria or the medium is not required to obtain CaRC. In contrast, calcium uptake capacity (CaUC) includes the correction for

incomplete $Ca^{2+}$ uptake determined by measurement of $Ca^{2+}$ concentrations in the incubation medium.

The term calcium uptake capacity (CaUC) was introduced in a study calibrating the CaG signal in the presence of mitochondrial preparations inhibited by rotenone or rotenone plus oligomycin (72). Apart from addressing the nomenclature, Murphy et al (1996) (72) corrected $Ca^{2+}$ uptake by the change of extramitochondrial $Ca^{2+}$ concentration. Even when this publication has been cited, only a few studies followed their guidelines in terms of correction for incomplete $Ca^{2+}$ uptake (68, 73). The majority of publications citing the method of Murphy et al did not present the CaUC, and the terms calcium uptake capacity and calcium retention capacity are frequently used to refer to the same result (74). This is particularly the case when the fluorescence signal is not calibrated, and the results are only calculated as the cumulative concentration of $Ca^{2+}$ added (31) or shown as representative traces with arbitrary units (75). Even when the $Ca^{2+}$ signal is calibrated, clarification may be missing if the calcium retention capacity reported refers to the CaUC or only to the cumulative $Ca^{2+}$ concentration added (CaRC) (59, 76). Methodological details on the optical effect of the sample on $Ca^{2+}$ calibration are often ignored (60, 71, 77, 78), regardless of evidence that intracellular conditions significantly alter both the apparent $K_d$ and the spectral properties of $Ca^{2+}$ indicators (26, 51, 79, 80).

Our results show that CaUC is underestimated by 45 and 55 % in controls and CsA treatments, respectively, compared to CaRC. This ambiguity combined with different experimental conditions leads to a high variability between studies (25). The intra-experimental calibration method introduced in the present study improves accuracy by accounting for the effect of sample on the optical signal and variability of calibration factors. Importantly, a clear distinction between calcium retention and uptake capacities improves reproducibility and comparability.

The proportion of CaUC to CaRC was different in controls compared to CsA. CsA induced an apparent increase in $Ca^{2+}$ uptake over the same number of $Ca^{2+}$ titrations as in controls. However, CsA had no effect on $Ca^{2+}$ uptake in individual $Ca^{2+}$ titrations, in accordance with a previous report showing the same $Ca^{2+}$ uptake rate for controls and CsA (68). CsA and, therefore, CypD, are not related to the $Ca^{2+}$ uptake process via MCU, as observed in studies using CypD-deficient mice (74, 75, 81, 82). Moreover, the CsA-CypD interaction correlates only with the retained $Ca^{2+}$ in the matrix, as quantified by CaUC, rather than with the total $Ca^{2+}$ added to the assay (CaRC).

Respiration increases transiently after $Ca^{2+}$ titrations (10, 50, 83, 84). This is due to $Ca^{2+}$ cycling stimulated by incomplete $Ca^{2+}$ uptake and correspondingly increased $Ca^{2+}$ concentrations in the medium, as shown by the reversibility of $Ca^{2+}$-stimulated leak respiration when the $Ca^{2+}$ concentration is reduced by addition of EGTA (84). Towards mtPT the respiration increases particularly in the presence of CsA, indicating higher proton leak which may result from mtPT pore opening in a subpopulation of mitochondria (21).

Calibration of the CaG signal as a function of $Ca^{2+}$ concentration (after inhibition of $Ca^{2+}$ uptake) is a widespread procedure (72, 86, 87), and it is also applied for

calibration of the fluorophore MgG (40). However, this approach resulted in calculated peak $Ca^{2+}$ concentrations that were higher than expected from the titrations of $Ca^{2+}$ under the present experimental conditions. The intra-experimental calibration avoids this artefact and, importantly, does not require separate experimental tests with mitochondria and inhibitors such as RR. Based on our previously published preprint (88) our calibration method was already applied (89).

The present method offers advantages of monitoring calcium dynamics and respiration simultaneously in the same chamber. The specifically modified incubation medium MiRCa was already applied in a collaborative study where it is called calcium respiration medium (33). The fluorescent dyes safranin, rhodamine and Amplex Red used to measure mtMP and hydrogen peroxide production can alter mitochondrial respiration (34, 35, 90, 91). In contrast, Magnesium Green (MgG), used to measure ATP production does not affect respiration (40). Similarly, CaG did not inhibit respiration.

By assessing $Ca^{2+}$ dynamics and respiration simultaneously in the Oroboros, any possible deviations are eliminated of titration regimes and experimental conditions in the multisensory measurements, compared to measuring $Ca^{2+}$ and respiration in different instruments (10, 92). The $Ca^{2+}$ retention capacity method using conventional spectrofluorometry in cuvettes with constant stirring has a low throughput compared to the Oroboros chambers, as only one cuvette is read at one time. The measurement of CaG in a plate reader increases the throughput, but it lacks the homogenization of the sample in media. Besides, recording must be interrupted by removing the plate for each $Ca^{2+}$ titration.

Although the volume of the Oroboros chambers (2 mL) is relatively high, the sample concentration is lower than commonly used in conventional spectrofluorometry. Many studies with isolated mitochondria use higher protein concentrations compared to the present study (54, 56, 71). At mitochondrial protein concentrations >0.2 $mg \cdot mL^{-1}$, the difference between CaUC and CaRC declined to c. 50 $nmol \cdot mg^{-1}$ but increased steeply <0.2 $mg \cdot mL^{-1}$ (Figure 6e). Low sample concentrations are frequently used with high-resolution respirometry and recommended in CaG assays to avoid frequent reoxygenations, which requires intermittent opening and closing the chambers which interrupts the measurements. The fact that CaRC, but not CaUC, depends on experimental mt-protein concentration supports the argument that the concept of the CaUC is superior to CaRC.

The use of isolated mitochondria in the CaG assay avoids the complexity of interactions with other organelles in calcium handling. Despite this advantage, isolated mitochondria may not fully recapitulate the complexity of living cells or tissues. Furthermore, the use of CaG restricts its application to mitochondrial preparations (isolated mitochondria, permeabilized cells and tissues) since the dye does not effectively permeate the plasma membrane. Consequently, this approach cannot be directly extended to living cells or intact tissues, where calcium signaling is regulated by additional compartments and mechanisms. Using permeabilized cells and

permeabilized tissues, which better preserve the structural and regulatory context of mitochondria compared to isolated organelles, broadens the physiological relevance while maintaining control over the intracellular environment.

We validated the method developed for isolated mitochondria with permeabilized cells. As in imt, the CaUC was lower than CaRC and the effect of CsA was more pronounced on CaUC than CaRC. A concern in studies with permeabilized cells is that $Ca^{2+}$ can be taken up by the ER/SR. To address this, thapsigargin, an inhibitor of SERCA (90), which is responsible for $Ca^{2+}$ uptake by ER/SR, can be used (93). SERCA is an ATP-dependent $Ca^{2+}$ ATPase, and therefore in the absence of ATP, as in the present experimental conditions, the CaRC and CaUC are not influenced by ER $Ca^{2+}$ uptake. This is consistent with previous reports based on measurements in the absence of ATP, using different experimental conditions (55, 70), in the presence of antimycin A (72), or the MCU inhibitor RR (68). $Ca^{2+}$ uptake in permeabilized cells with ATP allows for evaluation of the influence of ER/SR using thapsigargin. In this context, however, it must be considered that thapsigargin is also an ER/SR stressor and cell death inducer (94).

While a low concentration of ADP stimulates $Ca^{2+}$ uptake (44), higher concentrations of ADP or ATP inhibit or delay the mtPT (16, 22, 46, 95). ADP and ATP at 0.1-0.25 mM inhibit mtPT in brain (46) and liver mitochondria (96). Whereas CsA increased the $Ca^{2+}$-threshold for mtPT two-fold under the present experimental conditions, physiological concentrations of ATP in the incubation medium exerted a much more dramatic effect on increasing this $Ca^{2+}$-threshold. This observation must be considered when assessing the physiological relevance of mtPT (47) and the pharmacological effect of CsA.

Quantification of mitochondrial $Ca^{2+}$ uptake is essential for understanding its dual role in cellular metabolism and death signaling; however, the lack of standardized experimental procedures across laboratories hampers reproducibility and limits meaningful data comparison. Establishing quality-controlled protocols is critical to advance both basic research and therapeutic development in $Ca^{2+}$-mediated mitochondrial function. In addition, calculation of the actual CaUC, instead of CaRC provides reliable results and is essential for comparability and reproducibility. The calibration method presented in our study enables accurate quantification of $Ca^{2+}$ uptake by mitochondria without the need for external calibration procedures, thereby reducing sample requirements and streamlining experimental workflow. Using a medium developed for $Ca^{2+}$ measurements without negative impact on respiratory capacities ensures that experimental conditions do not interfere with mitochondrial function.

Application of the CaUC concept will improve our understanding of tissue-specific mitochondrial calcium handling in investigations of disease models characterized by altered calcium homeostasis.

## Abbreviations

The abbreviations used are: CaG, Calcium Green; CaRC, calcium retention capacity; CaUC, calcium uptake capacity; ce, cells; CsA, Cyclosporin A; ER, endoplasmic reticulum; ET, electron transfer; FBS, fetal bovine serum; *FCR,* flux control ratio; HRR, high-resolution respirometry; imt, isolated mitochondria; MgG, Magnesium Green; mtIM, mitochondrial inner membrane; MCU, mitochondrial calcium uniporter; mtMP, mitochondrial membrane potential; mtPT, mitochondrial permeability transition; MiRCa, mitochondrial respiration and calcium medium; MiR05, mitochondrial respiratiom medium; NCLX, $Na^+/Ca^{2+}/Li^+$ exchanger; OXPHOS, oxidative phosphorylation; POS, polarographic oxygen sensor; *ren*, residual endogenous substrates; *rox*, residual oxygen consumption; RR, ruthenium red; SR, sarcoplasmic reticulum; SD, standard deviation; TIP2k, Titration-Injection microPump; VDAC, voltage-dependent anion channel

## Data availability

Data available Open Access: https://doi.org/10.5281/zenodo.21023755

## Supporting information

This article contains supporting information.

## Funding and additional information

This work was supported by project NextGen-O2k which has received funding from the European Union's Horizon 2020 research and innovation programme under grant agreement Nº 859770.

## Conflicts of interest

CC, LHDC, and MG are employees of Oroboros Instruments. EG is founder and CEO of Oroboros Instruments.

## References

1. Berridge, M. J., Lipp, P., and Bootman, M. D. (2000) The versatility and universality of calcium signalling. *Nat. Rev. Mol. Cell Biol*. **1**, 11-21
2. Clapham, D. E. (2007) Calcium signaling. *Cell* **131**, 1047-1058
3. Modesti, L., Danese, A., Vitto, V. A. M., Ramaccini, D., Aguiari, G., Gafà, R., Lanza, G., Giorgi, C., and Pinton, P. (2021) Mitochondrial $Ca^{2+}$ signaling in health, disease and therapy. *Cells* **10**, 1317
4. Duchen, M. R. (2004) Roles of mitochondria in health and disease. *Diabetes.* **53**, S96-S102
5. Giorgi, C., Marchi, S., and Pinton, P. (2018) The machineries, regulation and cellular functions of mitochondrial calcium. *Nat. Rev. Mol. Cell Biol.* **19**, 713-730
6. McCormack, J. G., Halestrap, A. P., and Denton, R. M. (1990) Role of calcium ions in regulation of mammalian intramitochondrial metabolism. *Physiol. Rev*. **70**, 391-425
7. Balaban, R. S. (2009) The role of $Ca^{2+}$ signaling in the coordination of mitochondrial ATP production with cardiac work. *Biochim. Biophys. Acta Bioenerg*. **1787**, 1334-1341
8. Denton, R. M. (2009) Regulation of mitochondrial dehydrogenases by calcium ions. *Biochim. Biophys. Acta Bioenerg*. **1787**, 1309-1316
9. Vinnakota, K. C., Dash, R. K., and Beard, D. A. (2011) Stimulatory effects of calcium on respiration and NAD(P)H synthesis in intact rat heart mitochondria utilizing physiological substrates cannot explain respiratory control *in vivo*. *J. Biol. Chem*. **286**, 30816-30822

10. Vilas-Boas, E. A., Cabral-Costa, J. V., Ramos, V. M., Caldeira da Silva, C. C., and Kowaltowski, A. J. (2023) Goldilocks calcium concentrations and the regulation of oxidative phosphorylation: too much, too little, or just right. *J. Biol. Chem*. **299**, 102904
11. Marchi, S., and Pinton, P. (2014) The mitochondrial calcium uniporter complex: molecular components, structure and physiopathological implications. *J. Physiol*. **592**, 829-839
12. Carvalho, E. J., Stathopulos, P. B., and Madesh, M. (2020) Regulation of $Ca^{2+}$ exchanges and signaling in mitochondria. *Curr. Opin. Physiol*. **17**, 197-206
13. De Mario, A., D'Angelo, D., Zanotti, G., Raffaello, A., and Mammucari, C. (2023) The mitochondrial calcium uniporter complex—a play in five acts. *Cell Calcium.* **114**, 102720
14. Duvvuri, B., and Lood, C. (2021) Mitochondrial calcification. *Immunometabolism.* **3**, e210008
15. Carraro, M., and Bernardi, P. (2023) The mitochondrial permeability transition pore in $Ca^{2+}$ homeostasis. *Cell Calcium*. **111**, 102719
16. Bernardi, P., Gerle, C., Halestrap, A. P., Jonas, E. A., Karch, J., Mnatsakanyan, N., Pavlov, E., Sheu, S. S., and Soukas, A. A. (2023) Identity, structure, and function of the mitochondrial permeability transition pore: controversies, consensus, recent advances, and future directions. *Cell Death Differ*. **30**, 1869-1885
17. Griffiths, E. J., and Halestrap, A. P. (1993) Protection by cyclosporin A of ischemia/reperfusion-induced damage in isolated rat hearts. *J. Mol. Cell. Cardiol*. **25**, 1461-1469
18. Halestrap, A. P., Connern, C. P., Griffiths, E. J., and Kerr, P. M. (1997) Cyclosporin A binding to mitochondrial cyclophilin inhibits the permeability transition pore and protects hearts from ischaemia/reperfusion injury. *Mol. Cell. Biochem*. **174**, 167-172
19. Mather, M. W., and Rottenberg, H. (2002) The inhibition of calcium signaling in T lymphocytes from old mice results from enhanced activation of the mitochondrial permeability transition pore. *Mech. Ageing Dev*. **123**, 707-724
20. Du, H., Guo, L., Zhang, W., Rydzewska, M., and Yan, S. (2011) Cyclophilin D deficiency improves mitochondrial function and learning/memory in aging Alzheimer disease mouse model. *Neurobiol. Aging.* **32**, 398-406
21. Bernardi, P., Rasola, A., Forte, M., and Lippe, G. (2015) The mitochondrial permeability transition pore: channel formation by F-ATP synthase, integration in signal transduction, and role in pathophysiology. *Physiol. Rev*. **95**, 1111-1155
22. Tommasin, L., Carrer, A., Boscolo Nata, F., Frigo, E., Fogolari, F., Lippe, G., Carraro, M., and Bernardi, P. (January 14, 2025) Adenine nucleotide translocator and ATP synthase cooperate in mediating the mitochondrial permeability transition. *J. Physiol.* 10.1113/JP287147
23. Giorgio, V., von Stockum, S., Antoniel, M., Fabbro, A., Fogolari, F., Forte, M., Glick, G. D., Petronilli, V., Zoratti, M., Szabó, I., Lippe, G., and Bernardi, P. (2013) Dimers of mitochondrial ATP synthase form the permeability transition pore. *Proc. Natl. Acad. Sci. U. S. A.* **110**, 5887-5892
24. Carroll, J., He, J., Ding, S., Fearnley, I. M., and Walker, J. E. (2019) Persistence of the permeability transition pore in human mitochondria devoid of an assembled ATP synthase. *Proc. Natl. Acad. Sci. U. S. A*. **116**, 12816-12821
25. Endlicher, R., Drahota, Z., Štefková, K., Červinková, Z., and Kučera, O. (2023) The mitochondrial permeability transition pore—current knowledge of its structure, function, and regulation, and optimized methods for evaluating its functional state. *Cells*. **12**, 1273
26. Thermo Fischer Scientific (2010) Indicators for $Ca^{2+}$, $Mg^{2+}$, $Zn^{2+}$ and other metal ions. in *Molecular Probes Handbook, A Guide to Fluorescent Probes and Labeling Technologies,* 11th Ed. Thermo Fischer Scientific
27. Bernardi, P., Petronilli, V., Di Lisa, F., and Forte, M. (2001) A mitochondrial perspective on cell death. *Trends Biochem. Sci*. **26**, 112–117

28. Nászai, A., Terhes, E., Kaszaki, J., Boros, M., and Juhász, L. (2019) Ca($^{2+}$)N it be measured? Detection of extramitochondrial calcium movement with high-resolution FluoRespirometry. *Sci. Rep.* **9**, 19229
29. Spinazzi, M., Radaelli, E., Horré, K., Arranz, A. M., Gounko, N. V., Agostinis, P., Maia, T. M., Impens, F., Morais, V. A., Lopez-Lluch, G., Serneels, L., Navas, P., and De Strooper, B. (2019) PARL deficiency in mouse causes Complex III defects, coenzyme Q depletion, and Leigh-like syndrome. *Proc. Natl. Acad. Sci. U. S. A*. **116**, 277-286
30. Deline, M. L., Grashei, M., van Heijster, F. H. A., Schilling, F., Straub, J., and Fromme, T. (2021) Adenylate kinase derived ATP shapes respiration and calcium storage of isolated mitochondria. *Biochim. Biophys. Acta Bioenerg.* **1862**, 148409
31. Ahn, B., Ranjit, R., Kneis, P., Xu, H., Piekarz, K. M., Freeman, W. M., Kinter, M., Richardson, A., Ran, Q., Brooks, S. V., and Van Remmen, H. (2022) Scavenging mitochondrial hydrogen peroxide by peroxiredoxin 3 overexpression attenuates contractile dysfunction and muscle atrophy in a murine model of accelerated sarcopenia. *Aging Cell*. **21**, e13569
32. Xu, H., Ahn, B., and Van Remmen, H. (2022) Impact of aging and oxidative stress on specific components of excitation contraction coupling in regulating force generation. *Sci. Adv.* **8**, eadd7377
33. Donnelly, C., Komlódi, T., Cecatto, C., Cardoso, L. H. D., Compagnion, A. C., Matera, A., Tavernari, D., Campiche, O., Paolicelli, R. C., Zanou, N., Kayser, B., Gnaiger, E., and Place, N. (2024) Functional hypoxia reduces mitochondrial calcium uptake. *Redox Biol*. **71**, 103037
34. Krumschnabel, G., Eigentler, A., Fasching, M., and Gnaiger, E. (2014) Use of safranin for the assessment of mitochondrial membrane potential by high-resolution respirometry and fluorometry. *Methods Enzymol*. **542**, 163-181
35. Makrecka-Kuka, M., Krumschnabel, G., and Gnaiger, E. (2015) High-resolution respirometry for simultaneous measurement of oxygen and hydrogen peroxide fluxes in permeabilized cells, tissue homogenate and isolated mitochondria. *Biomolecules.* **5**, 1319-1338
36. Fontana-Ayoub, M., Fasching, M., and Gnaiger, E. (2016) Selected media and chemicals for respirometry with mitochondrial preparations. MiPNet03.02, Mitochondrial Physiology Network 02, 1-9 https://wiki.oroboros.at/images/3/3c/MiPNet03.02_Chemicals-Media.pdf
37. Baglivo, E., Cardoso, L. H. D., Cecatto, C., and Gnaiger, E. (2024) Stability of mitochondrial respiration medium used in high-resolution respirometry with living and permeabilized cells. *Bioenerg. Commun*. 10.26124/bec.2024-0008
38. Komlodi, T., Cardoso, L. H. D., Doerrier, C., and Gnaiger, E. (2021) Coupling and pathway control of coenzyme Q redox state and respiration in isolated mitochondria. *Bioenerg. Commun*. 10.26124/bec:2021-0003
39. Lassnig, B., and Gnaiger, E. (2010) Laboratory protocol: isolation of rat liver mitochondria. MiPNet08.13, Mitochondrial Physiology Network, 1-2 https://wiki.oroboros.at/images/9/93/MiPNet08.13_MitoIsolation-RLM.pdf
40. Cardoso, L. H. D., Doerrier, C., and Gnaiger, E. (2021) Magnesium Green for fluorometric measurement of ATP production does not interfere with mitochondrial respiration. *Bioenerg. Commun*. 10.26124/bec:2021-0001
41. Sailer, J., Schmitt, S., Zischka, H., and Gnaiger, E. (2025) Direct effects of clinically relevant antibiotics on mitochondrial respiration. *Int. J. Mol. Sci*. **26**, 5379
42. Baglivo, E., Cardoso, L. H. D., Cecatto, C., and Gnaiger, E. (2022) Statistical analysis of instrumental reproducibility as internal quality control in high-resolution respirometry. *Bioenerg. Commun*. 10.26124/bec:2022-0008
43. [preprint] Gnaiger, E., Cardoso, L. H. D., and MitoEAGLE Task Group (2025) Mitochondrial physiology, 2nd Ed. *BEC preprints*. 10.26124/becprep.2025-0006.ed2

44. Rottenberg, H., and Marbach, M. (1990) Regulation of $Ca^{2+}$ transport in brain mitochondria. II. The mechanism of the adenine nucleotides enhancement of $Ca^{2+}$ uptake and retention. *Biochim. Biophys. Acta. Bioenerg*. **1016**, 87-98
45. Williams, S. P., Fulton, A. M., and Brindle, K. M. (1993) Estimation of the intracellular free ADP concentration by fluorine-19 NMR studies of fluorine-labeled yeast phosphoglycerate kinase *in vivo*. *Biochemistry*. **32**, 4895-4902
46. Saito, A., and Castilho, R. F. (2010) Inhibitory effects of adenine nucleotides on brain mitochondrial permeability transition. *Neurochem. Res*. **35**, 1667-1674
47. Vercesi, A. E., Castilho, R. F., Kowaltowski, A. J., de Oliveira, H. C. F., de Souza-Pinto, N. C., Figueira, T. R., and Busanello, E. N. B. (2018) Mitochondrial calcium transport and the redox nature of the calcium-induced membrane permeability transition. *Free Radic. Biol. Med*. **129**, 1-24
48. Gradl, L., Gradl, P., and Gnaiger, E. (2021) Titration-injection microPump TIP2k manual. MiPNet12.10. Mitochondrial Physiology Network. 1-20 https://www.bioblast.at/images/9/9c/OroM2.3_TIP2k.pdf
49. Gnaiger, E. (2001) Bioenergetics at low oxygen: dependence of respiration and phosphorylation on oxygen and adenosine diphosphate supply. *Respir. Physiol*. **128**, 277-297
50. Duong, Q. V., Hoffman, A., Zhong, K., Dessinger, M. J., Zhang, Y., and Bazil, J. N. (2020) Calcium overload decreases net free radical emission in cardiac mitochondria. *Mitochondrion* **51**, 126-139
51. Serna, J. D. C., Ramos, V. M., Cabral-Costa, J. V., Vilas-Boas, E. A., Amaral, A. G., Ohya, G., Caldeira da Silva, C. C., and Kowaltowski, A. J. (2022) Measuring mitochondrial $Ca^{2+}$ efflux in isolated mitochondria and permeabilized cells. Bioenerg. Commun. 10.26124/bec:2022-0007
52. Basso, E., Petronilli, V., Forte, M. A., and Bernardi, P. (2008) Phosphate is essential for inhibition of the mitochondrial permeability transition pore by cyclosporin A and by cyclophilin D ablation. *J. Biol. Chem*. **283**, 26307-26311
53. Doczi, J., Torocsik, B., Echaniz-Laguna, A., De Camaret, B. M., Starkov, A., Starkova, N., Gál, A., Molnár, M. J., Kawamata, H., Manfredi, G., Adam-Vizi, V., and Chinopoulos, C. (2016) Alterations in voltage-sensing of the mitochondrial permeability transition pore in ANT1-deficient cells. *Sci. Rep*. **6**, 26700
54. Li, W., Zhang, C., and Sun, X. (2018) Mitochondrial $Ca^{2+}$ retention capacity assay and $Ca^{2+}$-triggered mitochondrial swelling assay. *J. Vis. Exp*. **135**, e56236
55. Harisseh, R., Abrial, M., Chiari, P., Al-Mawla, R., Villedieu, C., Tessier, N., Bidaux, G., Ovize, M., and Gharib, A. (2019) A modified calcium retention capacity assay clarifies the roles of extra- and intracellular calcium pools in mitochondrial permeability transition pore opening. *J. Biol. Chem*. **294**, 15282-15292
56. Deak, A. T., Jean-Quartier, C., Bondarenko, A. I., Groschner, L. N., Malli, R., Graier, W. F., and Waldeck-Weiermair, M. (2021) Assessment of mitochondrial $Ca^{2+}$ uptake. In: Weissig, V., Edeas, M. (eds) *Mitochondrial Medicine. Methods in Molecular Biology*. **2276**. Springer, New York, NY.
57. Ghazal, N., and Kwong, J. Q. (2025) Analyzing mitochondrial calcium influx in isolated mitochondria. In: Gorvin, C.M. (eds) *Calcium Signaling. Methods in Molecular Biology*. **2861**. Humana, New York, NY
58. Chinopoulos, C., Kiss, G., Kawamata, H., and Starkov, A. A. (2014) Measurement of ADP-ATP exchange in relation to mitochondrial transmembrane potential and oxygen consumption. *Methods Enzymol*. **542**, 333-348
59. Amigo, I., Menezes-Filho, S. L., Luévano-Martínez, L. A., Chausse, B., and Kowaltowski, A. J. (2017) Caloric restriction increases brain mitochondrial calcium retention capacity and protects against excitotoxicity. *Aging Cell.* **16**, 73-81
60. Cefis, M., Marcangeli, V., Hammad, R., Granet, J., Leduc-Gaudet, J. P., Gaudreau, P., Trumpff, C., Huang, Q., Picard, M., Aubertin-Leheudre, M., Bélanger, M., Robitaille, R., Morais, J. A., and Gouspillou, G. (2025) Impact of physical activity on physical function,

mitochondrial energetics, ROS production, and $Ca^{2+}$ handling across the adult lifespan in men. *Cell Rep. Med*. **6**, 101968
61. Wollenman, L. C., Vander Ploeg, M. R., Miller, M. L., Zhang, Y., and Bazil, J. N. (2017) The effect of respiration buffer composition on mitochondrial metabolism and function. *PLoS One.* **12**, e0187523
62. Doerrier, C., Gama-Perez, P., Pesta, D., Distefano, G., Soendergaard, S. D., Chroeis, K. M., Gonzalez-Franquesa, A., Goodpaster, B. H., Prats, C., Sales-Pardo, M., Guimera, R., Coen, P. M., Gnaiger, E., Larsen, S., and Garcia-Roves, P. M. (2024) Harmonization of experimental procedures to assess mitochondrial respiration in human permeabilized skeletal muscle fibers. *Free Radic. Biol. Med*. **223**, 384-397
63. Monteiro, J., Assis-de-Lemos, G., de-Souza-Ferreira, E., Marques, A. M., Neves, G. A., Silveira, M. S., and Galina, A. (2020) Energization by multiple substrates and calcium challenge reveal dysfunctions in brain mitochondria in a model related to acute psychosis. *J. Bioenerg. Biomembr*. **52**, 1-15
64. Drahota, Z., Endlicher, R., Kučera, O., Rychtrmoc, D., and Červinková, Z. (2020) Factors affecting the function of the mitochondrial membrane permeability transition pore and their role in evaluation of calcium retention capacity values. *Physiol. Res*. **69**, 491-499
65. Csordás, G., Thomas, A. P., and Hajnóczky, G. (1999) Quasi-synaptic calcium signal transmission between endoplasmic reticulum and mitochondria. *EMBO J*. **18**, 96-108
66. Rizzuto, R., De Stefani, D., Raffaello, A., and Mammucari, C. (2012) Mitochondria as sensors and regulators of calcium signalling. *Nat. Rev. Mol. Cell Biol*. **13**, 566-578
67. Chalmers, S., and Nicholls, D. G. (2003) The relationship between free and total calcium concentrations in the matrix of liver and brain mitochondria. *J. Biol. Chem.* **278**, 19062-19070
68. Kowaltowski, A. J., Menezes-Filho, S. L., Assali, E. A., Gonçalves, I. G., Cabral-Costa, J. V., Abreu, P., Miller, N., Nolasco, P., Laurindo, F. R. M., Bruni-Cardoso, A., and Shirihai, O. S. (2019) Mitochondrial morphology regulates organellar $Ca^{2+}$ uptake and changes cellular $Ca^{2+}$ homeostasis. *FASEB J.* **33**, 13176–13188
69. Bernardi, P., Krauskopf, A., Basso, E., Petronilli, V., Blalchy-Dyson, E., Di Lisa, F., and Forte, M. A. (2006) The mitochondrial permeability transition from *in vitro* artifact to disease target. *FEBS J.* **273**, 2077–2099
70. Jang, S., Chapa-Dubocq, X. R., Fossati, S., and Javadov, S. (2021) Analysis of Mitochondrial Calcium Retention Capacity in Cultured Cells: Permeabilized Cells Versus Isolated Mitochondria. *Front. Physiol.* **12**, 773839
71. Mendoza, A. M., and Karch, J. (2022) Simultaneous Acquisition of Mitochondrial Calcium Retention Capacity and Swelling to Measure Permeability Transition Sensitivity. In: Tomar, N. (eds) *Mitochondria. Methods in Molecular Biology*. **2497**. Humana, New York, NY
72. Murphy, A. N., Bredesen, D. E., Cortopassi, G., Wang, E., and Fiskum, G. (1996) Bcl-2 potentiates the maximal calcium uptake capacity of neural cell mitochondria. *Proc. Natl. Acad. Sci. U. S. A.* **93**, 9893–9898
73. Bambrick, L. L., Chandrasekaran, K., Mehrabian, Z., Wright, C., Krueger, B. K., and Fiskum, G. (2006) Cyclosporin A increases mitochondrial calcium uptake capacity in cortical astrocytes but not cerebellar granule neurons. *J. Bioenerg. Biomembr.* **38**, 43–47
74. Hamilton, J., Brustovetsky, T., and Brustovetsky, N. (2021) The effect of mitochondrial calcium uniporter and cyclophilin D knockout on resistance of brain mitochondria to $Ca^{2+}$-induced damage. *J. Biol. Chem.* **296**, 100669
75. Perry, G. M., Tallaksen-Greene, S., Kumar, A., Heng, M. Y., Kneynsberg, A., van Groen, T., Detloff, P. J., Albin, R. L., and Lesort, M. (2010) Mitochondrial calcium uptake capacity as a therapeutic target in the R6/2 mouse model of Huntington's disease. *Hum. Mol. Genet.* **19**, 3354–3371

76. Bellissimo, C. A., Soendergaard, S., and Perry, C. G. R. (2023) The influence of adenylate cycling on mitochondrial calcium-induced permeability transition in permeabilized skeletal muscle fibers. *Bioenerg. Commun.* 10.26124/bec:2023-0001
77. Fontaine, E., Eriksson, O., Ichas, F., and Bernardi, P. (1998) Regulation of the permeability transition pore in skeletal muscle mitochondria modulation by electron flow through the respiratory chain complex I. *J. Biol. Chem.* **273**, 12662–12668
78. Picard, M., Csukly, K., Robillard, M.E., Godin, R., Ascah, A., Bourcier-Lucas, C., and Burelle, Y. (2008) Resistance to $Ca^{2+}$-induced opening of the permeability transition pore differs in mitochondria from glycolytic and oxidative muscles. *Am. J. Physiol. Regul. Integr. Comp. Physiol.* **295**, R659–R668
79. Takahashi, A., Camacho, P., Lechleiter, J. D., and Herman, B. (1999) Measurement of Intracellular Calcium. *Physiol Rev.* **79**, 1189–1125
80. Paredes, R. M., Etzler, J. C., Watts, L. T., Zheng, W., and Lechleiter, J. D. (2008) Chemical calcium indicators. *Methods*. **46**, 143–151
81. Baines, C. P., Kaiser, R. A., Purcell, N. H., Blair, N. S., Osinska, H., Hambleton, M. A., Brunskill, E. W., Sayen, M. R., Gottlieb, R. A., Dorn, G. W., Bobbins, J., and Molkentin, J. D. (2005) Loss of cyclophilin D reveals a critical role for mitochondrial permeability transition in cell death. *Nature*. **434**, 658–662
82. Elrod, J. W., Wong, R., Mishra, S., Vagnozzi, R. J., Sakthievel, B., Goonasekera, S. A., Karch, J., Gabel, S., Farber, J., Force, T., Brown, J. H., Murphy, E., and Molkentin, J. D. (2010) Cyclophilin D controls mitochondrial pore-dependent $Ca^{2+}$ exchange, metabolic flexibility, and propensity for heart failure in mice. *J. Clin. Invest.* **120**, 3680–3687
83. Walkon, L. L., Strubbe-Rivera, J. O., and Bazil, J. N. (2022) Calcium Overload and Mitochondrial Metabolism. *Biomolecules*. **12**, 1891
84. Strubbe-Rivera, J. O., Schrad, J. R., Pavlov, E. V., Conway, J. F., Parent, K. N., and Bazil, J. N. (2021) The mitochondrial permeability transition phenomenon elucidated by cryo-EM reveals the genuine impact of calcium overload on mitochondrial structure and function. *Sci. Rep.* **11**, 1037
85. Bernardi, P., and Pietrobon, D. (1982) On the nature of Pi-induced, $Mg^{2+}$-prevented $Ca^{2+}$ release in rat liver mitochondria. *FEBS Lett*. **139**, 9-12
86. Wei, A. C., Liu, T., Cortassa, S., Winslow, R. L., and O'Rourke, B. (2011) Mitochondrial $Ca^{2+}$ influx and efflux rates in guinea pig cardiac mitochondria: Low and high affinity effects of cyclosporine A. *Biochim. Biophys. Acta Mol. Cell Res.* **1813**, 1373–1381
87. Kristián, T., Gertsch, J., Bates, T. E., and Siesjö, B. K. (2000) Characteristics of the calcium-triggered mitochondrial permeability transition in nonsynaptic brain mitochondria: Effect of cyclosporin A and ubiquinone O. *J. Neurochem.* **74**, 1999–2009
88. [preprint] Cecatto, C., Cardoso, L. H. D., Grings, M., and Gnaiger, E. (2025) Mitochondrial $Ca^{2+}$ uptake and high-resolution respirometry. *BEC preprints*. 10.22024/bec.2025.01
89. Dalla Costa, A. P., Navarro, C. D. C., Siqueira-Santos, E. S., Velasco, R. Q. S., Rosada, J. V. F., Salgado, A. R., Demolin, D. M. R., Passos, L. A. C., Vercesi, A. E., Francisco, A., and Castilho, R. F. (2025) NNT deficiency alters cardiac structure and function without impairing mitochondrial bioenergetics in aged mice. *Redox Biol.* **88**, 103935
90. Scaduto, R. C., and Grotyohann, L. W. (1999) Measurement of mitochondrial membrane potential using fluorescent rhodamine derivatives. *Biophys. J.* **76**, 469–477
91. Davis, M., Barrett, M., Bayly, W., and Bollinger, A. (2024) Effect of selected fluorophores on equine skeletal muscle mitochondrial respiration. *Bioenerg. Commun.* 10.26124/bec:2024-0002
92. Szibor, M., Gizatullina, Z., Gainutdinov, T., Endres, T., Debska-Vielhaber, G., Kunz, M., Karavasili, N., Hallmann, K., Schreiber, F., Bamberger, A., Schwarzer, M., Doenst, T., Heinze, H. J., Lessmann, V., Vielhaber, S., Kunz, W. S., and Gellerich, F. N. (2020) Cytosolic, but not matrix, calcium is essential for adjustment of mitochondrial pyruvate supply. *J. Biol. Chem.* **295**, 4383–4397

93. McKenzie, M., Lim, S. C., and Duchen, M. R. (2017) Simultaneous Measurement of Mitochondrial Calcium and Mitochondrial Membrane Potential in Live Cells by Fluorescent Microscopy. *J. Vis. Exp.* **119**, 55166
94. Jaskulska, A., Janecka, A. E., and Gach-Janczak, K. (2021) Thapsigargin—from traditional medicine to anticancer drug. *Int. J. Mol. Sci.* **22**, 4
95. Chapa-Dubocq, X. R., Garcia-Baez, J. F., Bazil, J. N., and Javadov, S. (2023) Crosstalk between adenine nucleotide transporter and mitochondrial swelling: experimental and computational approaches. *Cell Biol. Toxicol.* **39**, 435–450
96. Vergun, O., and Reynolds, I. J. (2005) Distinct characteristics of $Ca^{2+}$-induced depolarization of isolated brain and liver mitochondria. *Biochim. Biophys. Acta Bioenerg.* **1709**, 127–137



## Supplementary material

### Supporting information A

### Polynomial calibration of [$Ca^{2+}$] – methods and arguments for rejection

Figure S1a shows a representative trace of a $Ca^{2+}$ calibration in the presence of mitochondria isolated from mouse liver and a cocktail containing rotenone, antimycin A, and the uncoupler CCCP. The second-order polynomial fit is shown in Figure S1b. The fluorescence signal increased linearly in the range from 3 nA to 5.5 nA (10 – 25 µM $Ca^{2+}$), but less steeply at higher $Ca^{2+}$ concentrations due to saturation of CaG.

The fluorescence calibration curves showed a pronounced right-shift from experimentally irrelevant tests without sample to calibrations in the presence of inhibited isolated mitochondria (Figure S1c). The presence of sample is essential to perform correct optical calibrations.

There was no difference in calibration curves when inhibiting $Ca^{2+}$ uptake either by the MCU inhibitor ruthenium red RR or by inhibiting the mitochondrial ETS and collapsing the protonmotive force *pmF* with the cocktail containing rotenone and antimycin A, plus the uncoupler CCCP (Figure S1d and S1e), except for one run (P7A, considered as an outlier). The first two $Ca^{2+}$ titrations resulted in high variability of the change in the fluorescence signal ($\Delta FS$) compared to the third and further titrations (Figure S1e). This can be explained by the variability of contaminant $Ca^{2+}$ concentrations, since identical concentrations of EGTA were used in all experimental tests, and thus might not be related to the method of inhibiting $Ca^{2+}$ uptake. Due to the difficulty of washing out the RR from the chambers, we recommend using the cocktail (Rot, Ama and CCCP), to avoid carry-over of RR to subsequent experiments. The more specific MCU inhibitor Ru360 can be considered but the carry-over effect was not evaluated in the present study. The effect of MCU inhibition by RR on mitochondrial

respiration is shown in Figure S2a. The transient increase of $O_2$ flux (Figures 3a, S5c and S6a) cannot be observed when MCU is inhibited. Of note, RR did not interfere significantly with the fluorescence signal in the absence of mitochondria (Figure S2b). Rot, Ama and CCCP were added after imt, allowing the sample's functionality to be assessed prior to inhibition. These compounds did not interfere with the CaG signal.

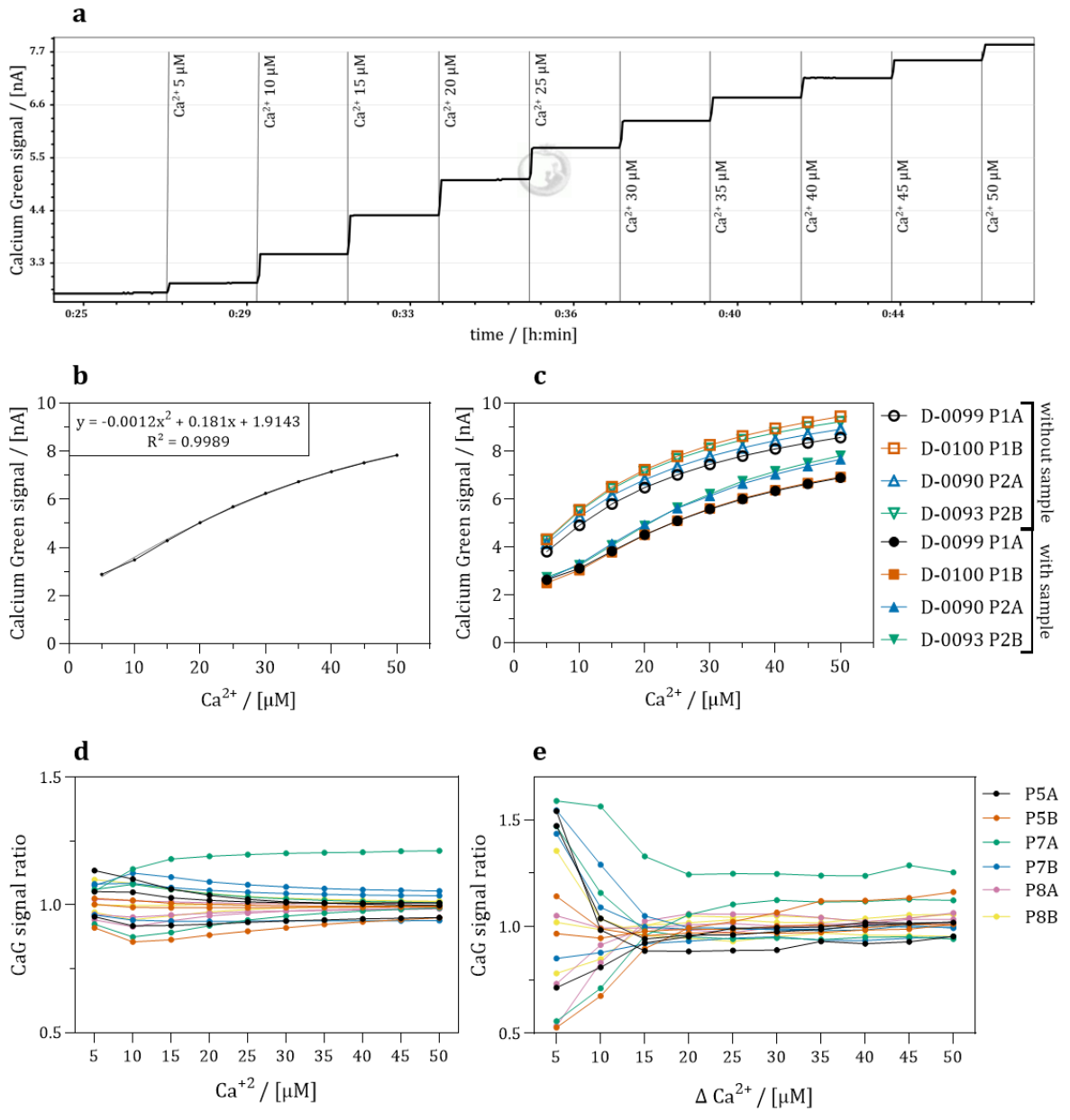


**Figure S1. Polynomial calcium calibration.** Calibration was performed in the same conditions as the experiment, in the presence of liver mitochondria and RR or cocktail of Rot+Ama+CCCP to inhibit $Ca^{2+}$ uptake. **(a)** Representative trace of Calcium Green (CaG) signal in $Ca^{2+}$ titrations. **(b)** Polynomial fit of the trace in panel a. Experiment: 2021-09-02 P3-03; Protocol: CaG (2 µM); G (10 mM); M (2 mM); ADP (30 µM); Omy (2.5 µM); EGTA (15 µM); imt; Rot (0.5 µM); Ama (2.5 µM); CCCP (1 µM); $Ca^{2+}$ (5 µM each). **(c)** Polynomial fits in the absence or presence of sample and RR (1 µM) to inhibit $Ca^{2+}$ uptake. Identical combinations

of chambers (Oroboros instrumental P number and letters A and B for the right and left chamber, respectively) and Fluo-Sensors (sensor-specific D-number) were used under experimental conditions. Open and closed symbols indicate experiments without and with sample, respectively. **(d)** CaG fluorescence signal measured after sequential 5 µM $Ca^{2+}$ titrations in the presence of RR divided by the corresponding signal in the presence of the cocktail Rot+Ama+CCCP. **(e)** Changes in the CaG fluorescence signal (Δ*FS*) in response to 5 µM $Ca^{2+}$ titrations ($\Delta Ca^{2+}$) in the presence of RR divided by the corresponding Δ*FS* in the presence of the cocktail. The same sample was used for calibration with RR or cocktail in 6 technical repeats on the same day (different colors) and the experiment was repeated on 3 different days (identical colors). Mt-protein concentration: 0.09 ± 0.008 mg·mL$^{-1}$.

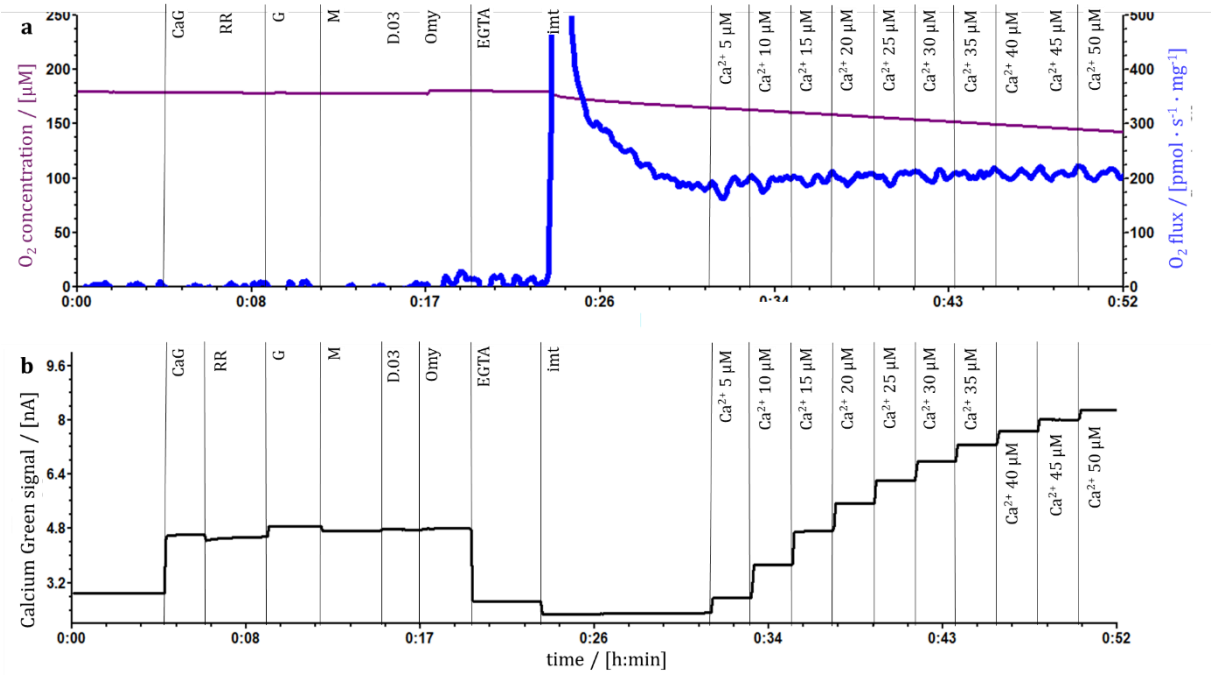


**Figure S2. Calcium titrations with ruthenium red (RR).** Calibration was performed under experimental conditions, in the presence of liver mitochondria and RR to inhibit $Ca^{2+}$ uptake. **(a)** Representative trace of $O_2$ consumption in $Ca^{2+}$ titrations with RR. $O_2$ concentration (purple line), $O_2$ flux (blue line). **(b)** Representative trace of Calcium Green (CaG) signal in $Ca^{2+}$ titrations. Experiment: 2021-03-30 P7-03; Protocol: CaG (2 µM); RR (1 µM); G (10 mM); M (2 mM); ADP (30 µM); Omy (2.5 µM); EGTA (15 µM); imt; $Ca^{2+}$ (5 µM each). *N* = 3. Mt-protein concentration: 0.087 ± 0.006 mg·mL$^{-1}$.

When comparing different samples using the same set of Fluo-Sensor and chamber, we observed that although there was a slight difference at higher [$Ca^{2+}$] using the same set in combination 1 (Figure S3a), in combination 2 (Figure S3b) the CaG signal was comparable on different days with different samples.

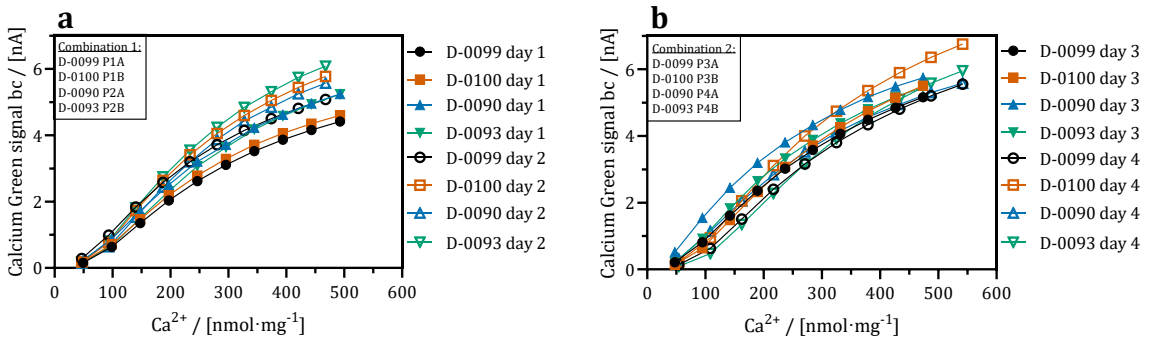


**Figure S3. Influence of sample preparation on $Ca^{2+}$ calibration.** Calibrations were performed under experimental conditions, in the presence of mitochondria isolated from mouse liver with $Ca^{2+}$ uptake inhibited by RR or Rot+Ama+CCCP. The same combination of chamber and Fluo-Sensor was used for comparison. **(a)** and **(b)** Polynomial fit baseline-corrected for *rox* with different sample preparations performed on different days. Baseline day 1: 2.453 ± 0.107; day 2: 2.411 ± 0.099; day 3: 2.565 ± 0.088; day 4: 2.572 ± 0.116 (nA, mean ± SD).

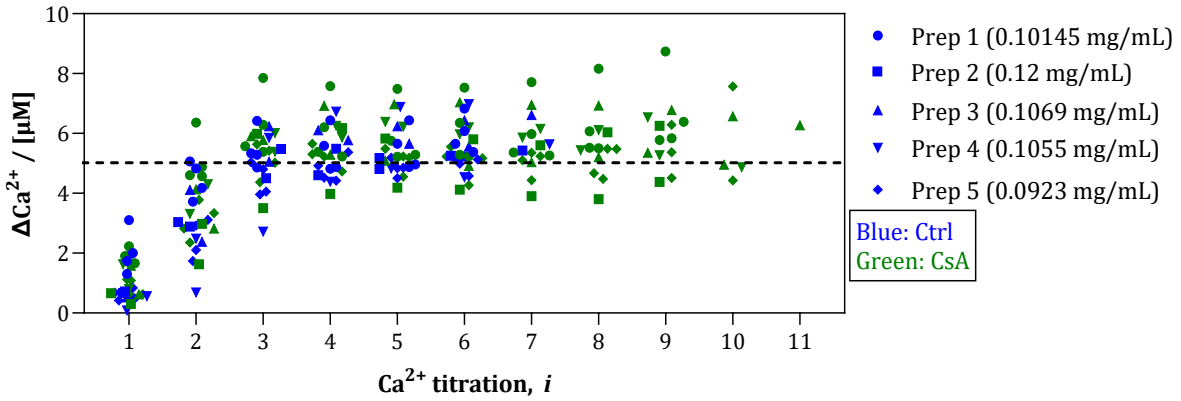


**Figure S4. Calcium concentration changes upon 5 µM $Ca^{2+}$ titrations during calcium uptake measurements calculated from polynomial fit calibrations.** Calibration curves were obtained immediately after the calcium uptake measurements on each sample and combination of Fluo-Sensor and Oroboros. Different symbols indicate independent sample preparations, each symbol indicates technical repeats, blue symbols represent Ctrl and green symbols CsA. Protocol: CaG (2 µM); G (10 mM); M (2 mM); ADP (30 µM); Omy (2.5 µM); EGTA (15 µM); imt; $Ca^{2+}$ (5 µM each). *N* = 5.

## Supporting information B

### Statistics for Figure 2

**Table S1. Specific $O_2$ flux: *p*-values summarized from Figure 2a:** Two-way repeated-measures ANOVA with Tukey's multiple comparison post-test. *p*-values correspond to pairwise comparisons between columns within each row. Analyzed by GraphPad10.4.

| Events | States | MiRCa vs. MiR05 | MiRCa+CaG vs. MiR05+CaG |
|---|---|---|---|
| 1mt | *ren* | 0.032 | 0.041 |
| 1PM | $N_L$ | 0.872 | 0.105 |
| 2D | $N_P$ | 0.312 | 0.016 |
| 2c | $Nc_P$ | 0.208 | 0.019 |
| 3G | $N_P$ | 0.068 | 0.697 |
| 4S | $NS_P$ | 0.823 | 0.621 |
| 5U | $NS_E$ | 0.922 | 0.878 |
| 6Rot | $S_E$ | 0.276 | 0.186 |
| 7Ama | *rox* | 0.525 | 0.210 |

**Table S2. Flux control ratio *FCR*: *p*-values summarized from Figure 2b:** Two-way mixed ANOVA with Tukey's multiple comparison post-test. *p*-values correspond to pairwise comparisons between columns within each row. Analyzed by GraphPad10.4.

| Events | States | MiRCa vs. MiR05 | MiRCa+CaG vs. MiR05+CaG |
|---|---|---|---|
| 1mt | *ren* | 0.103 | 0.092 |
| 1PM | $N_L$ | 0.551 | 0.162 |
| 2D | $N_P$ | 0.592 | 0.006* |
| 2c | $Nc_P$ | 0.555 | 0.002* |
| 3G | $N_P$ | 0.412 | 0.992 |
| 4S | $NS_P$ | 0.668 | 0.277 |
| 5U | $NS_E$ | - | - |
| 6Rot | $S_E$ | 0.006* | 0.006* |
| 7Ama | *rox* | 0.432 | 0.173 |

Footnote: asterisks (*) indicate low *p*-values.

**Table S3. Protein-specific $O_2$ flux: Combined *p*-values summarized from Figure 2a, considering that CaG has no effect**. Groups with CaG were integrated into the respective medium groups. Two-way repeated-measures ANOVA with Sidák's multiple comparison post-test. *p*-values correspond to pairwise comparisons between columns within each row. Analyzed by GraphPad10.4.

| Events | States | MiRCa and MiRCa+CaG vs. MiR05 and MiR05+CaG |
|---|---|---|
| 1mt | *ren* | >0.999 |
| 1PM | $N_L$ | >0.999 |
| 2D | $N_P$ | 0.996 |
| 2c | $Nc_P$ | 0.979 |
| 3G | $N_P$ | 0.736 |
| 4S | $NS_P$ | 0.009* |
| 5U | $NS_E$ | 0.621 |
| 6Rot | $S_E$ | 0.010* |
| 7Ama | *rox* | >0.999 |

Footnote: asterisks (*) indicate low *p*-values.

**Table S4. Flux control ratio *FCR*: Combined *p*-values summarized from Figure 2b, considering that CaG has no effect.** Groups with CaG were integrated into the respective medium groups. Two-way repeated-measures ANOVA with Sidák's multiple comparison post-test. *p*-values correspond to pairwise comparisons between columns within each row. Analyzed by GraphPad10.4.

| Events | States | MiRCa and MiRCa+CaG vs. MiR05 and MiR05+CaG |
|---|---|---|
| 1mt | *ren* | 0.998 |
| 1PM | $N_L$ | 0.999 |
| 2D | $N_P$ | 0.198 |
| 2c | $Nc_P$ | 0.038 |
| 3G | $N_P$ | 0.291 |
| 4S | $NS_P$ | 0.0002* |
| 5U | $NS_E$ | >0.999 |
| 6Rot | $S_E$ | <0.0001* |
| 7Ama | *rox* | >0.999 |

Footnote: asterisks (*) indicate low *p*-values.

## Supporting information C

## Continuous calcium titrations, titration steps, and carrier control

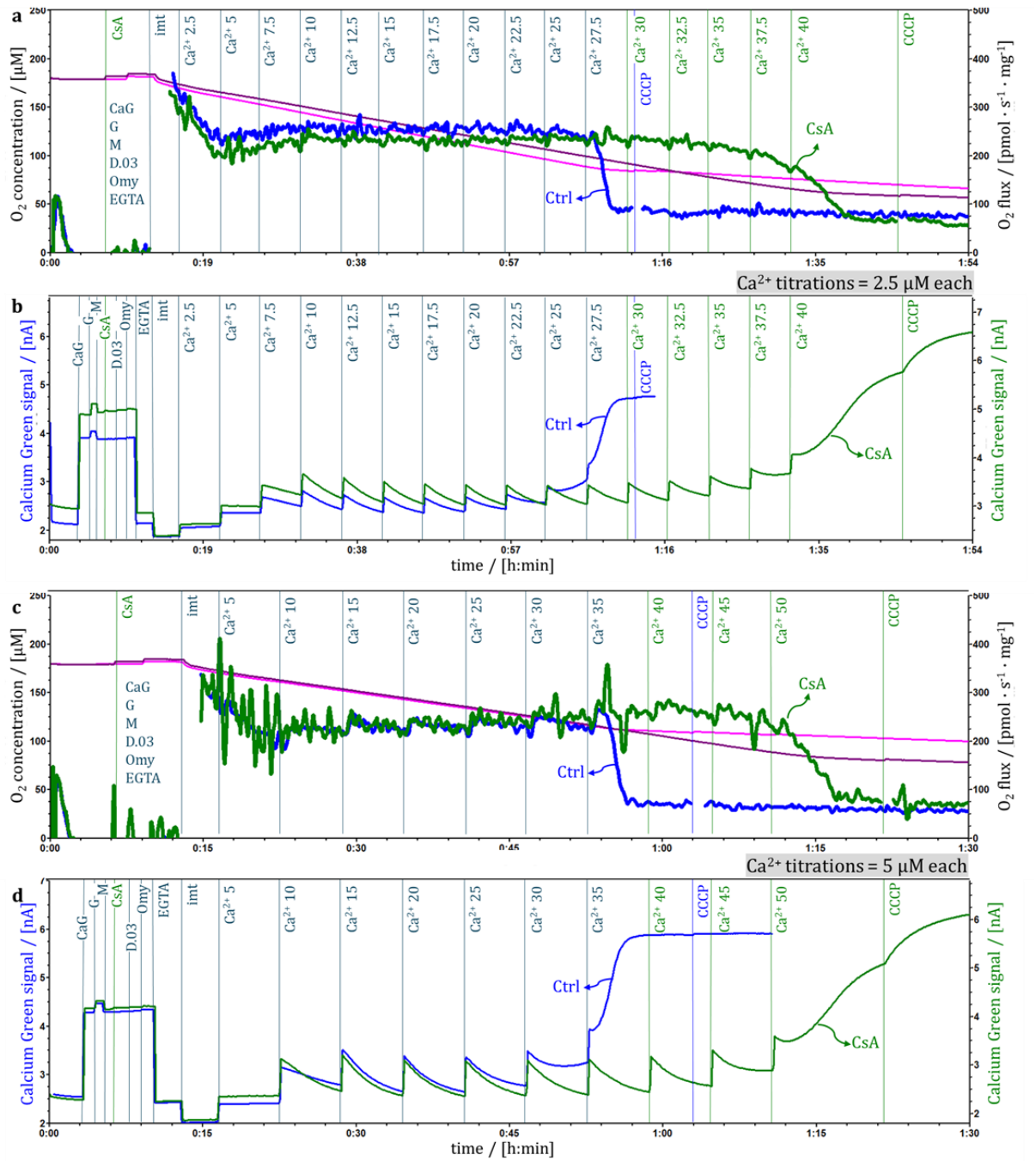


**Figure S5. Respiration and calcium uptake with 2.5 and 5 µM $Ca^{2+}$ titration steps.** Representative traces (protocol SUIT-035_CaG_D083) with glutamate (G, 10 mM) and malate (M, 2 mM) as substrates in the leak(Omy) state. Cyclosporin A (CsA, 1 µM), Calcium Green (CaG, 2 µM), ADP (D.03, 30 µM), Oligomycin (Omy, 20 nM), and EGTA (15 µM) added before isolated mitochondria (imt). Subsequently, $CaCl_2$ ($Ca^{2+}$) was titrated in steps of 2.5 µM (**a** and **b**) or 5 µM (**c** and **d**) (cumulative concentration stated in the vertical lines) until calcium release was observed as an increase in the CaG signal. Dark blue vertical lines represent events in

both chambers, lighter blue in chamber A and green in chamber B. **(a) (c)** $O_2$ concentration (pink and purple lines), specific $O_2$ flux in the absence (blue line, Ctrl) or presence of CsA (green line, CsA). **(b) (d)** CaG signal in the absence (blue line, Ctrl) or presence of CsA (green line, CsA). Experiments 2021-02-17 P7-02 and 2021-02-17 P8-02; *N* = 3; mt-protein concentration: 0.095 ± 0.016 mg·mL$^{-1}$.

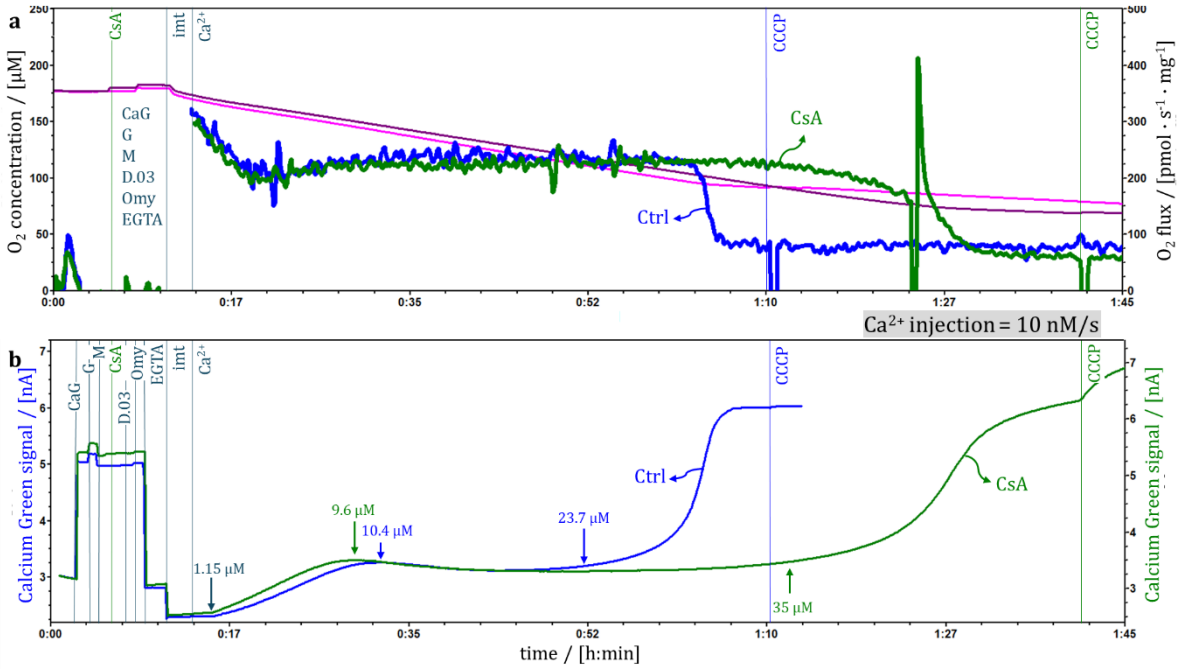


**Figure S6. Respiration and calcium uptake with continuous injection of $Ca^{2+}$.** Representative traces of the calcium injection protocol with glutamate (G, 10 mM) and malate (M, 2 mM) as substrates in the leak(Omy) state. Cyclosporin A (CsA, 1 µM), Calcium Green (CaG, 2 µM), ADP (30 µM), Oligomycin (Omy, 20 nM), and EGTA were added before isolated mitochondria (imt). Subsequently, $CaCl_2$ was injected by the TIP2k at a rate of 10 nM/s ($Ca^{2+}$) until calcium release was observed as an increase in the CaG signal. Dark blue vertical lines represent events in both chambers, blue in chamber A and green in chamber B. **(a)** $O_2$ concentration (pink and purple lines), specific $O_2$ flux in the absence (blue line, Ctrl) or presence of CsA (green line, CsA). **(b)** CaG signal in the absence (blue line, Ctrl) or presence of CsA (green line, CsA). The first arrow points to the experimental time until the cumulative injected $Ca^{2+}$ did not change the CaG signal (1.15 µM). The second pair of arrows points to the experimental time at the end of initial increase and beginning of the steady-state (cumulative injected $Ca^{2+}$ 9.6 µM and 10.4 µM). The last two arrows point to the experimental time when the CaG signal starts to increase, indicating mtPT (cumulative injected $Ca^{2+}$ 23.7 µM and 35 µM). Experiment 2021-02-17 P5-02. *N* = 3; mt-protein concentration: 0.095 ± 0.016 mg·mL$^{-1}$.

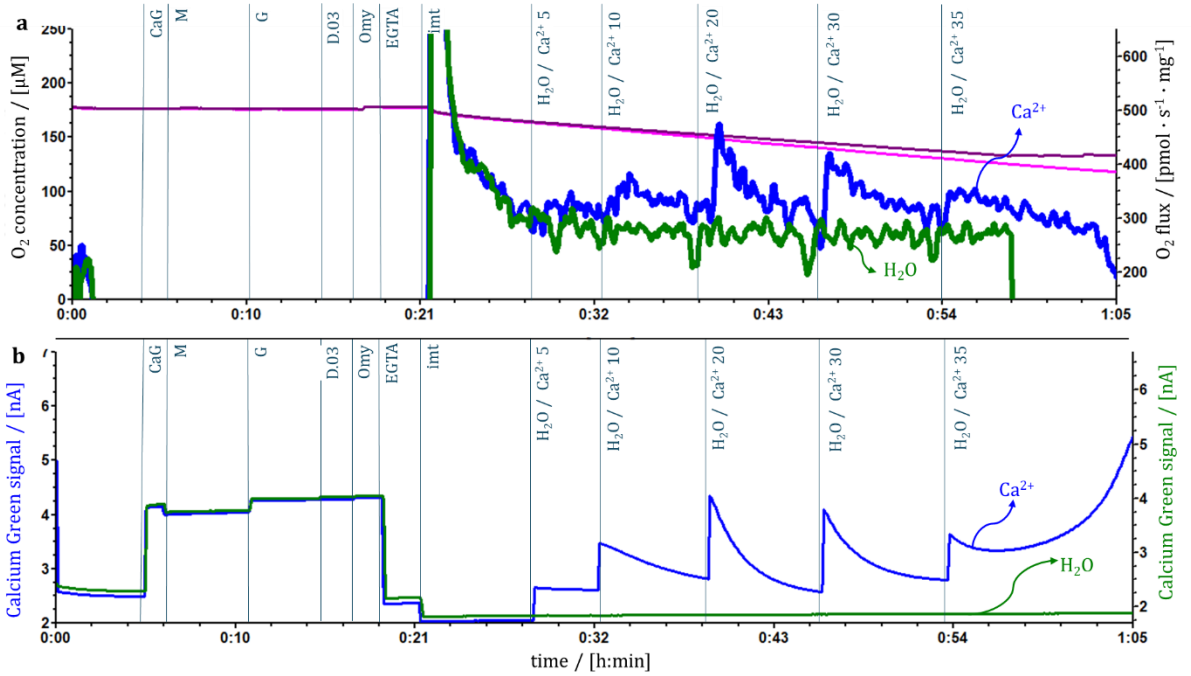


**Figure S7. Respiration and calcium uptake comparing steps of $Ca^{2+}$ titration and its carrier ($H_2O$).** Representative traces (protocol SUIT-035_CaG_D083) with glutamate (G, 10 mM) and malate (M, 2 mM) as substrates in the leak(Omy) state. Calcium Green (CaG, 2 µM), ADP (D.03, 30 µM), Oligomycin (Omy, 20 nM), and EGTA (15 µM) added before isolated mitochondria (imt). Subsequently, $CaCl_2$ ($Ca^{2+}$) or the carrier $H_2O$ were titrated in steps until calcium release was observed as an increase in the CaG signal in the chamber with $Ca^{2+}$ titrations. Dark blue vertical lines represent events in both chambers. **(a)** $O_2$ concentration (pink and purple lines), specific $O_2$ flux with $Ca^{2+}$ titrations (blue line, $Ca^{2+}$) or carrier (green line, $H_2O$). **(b)** CaG signal with $Ca^{2+}$ titrations (blue line, $Ca^{2+}$) or carrier (green line, $H_2O$). Experiment 2021-03-22 P8-02. *N* = 2; mt-protein concentration: 0.072 ± 0.013 mg·mL$^{-1}$.

## Supporting information D

### Different $O_2$ flux patterns during calcium uptake

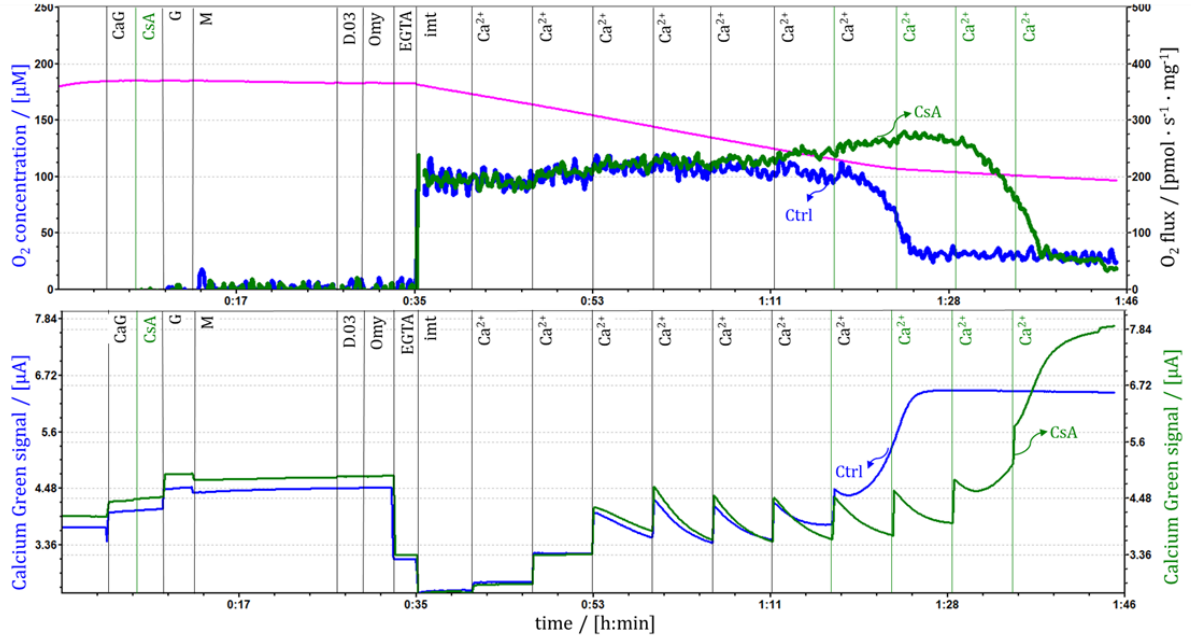


**Figure S8. Increase in leak respiration in the CsA group upon additional $Ca^{2+}$ titrations beyond mtPT in Ctrl.** Simultaneous measurements of respiration (upper graph) and calcium uptake (lower graph) by high-resolution respirometry with the Oroboros Fluo Smart-Module in mitochondria isolated from mouse liver. Representative trace for calcium uptake protocol (SUIT-035_CaG_D083) as described in Figure 3. Observed in 9 experimental runs with different mt-preparations. Experiment 2021-08-03 PQ1-04.

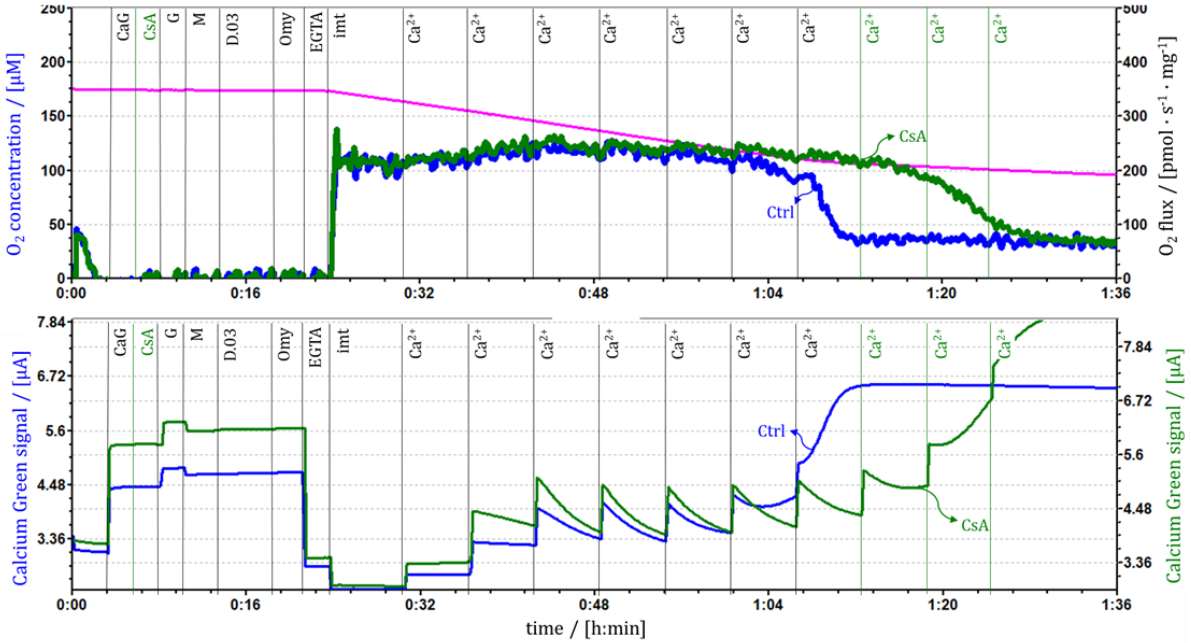


**Figure S9. CsA caused no increase in leak respiration.** Simultaneous measurements of respiration (upper graph) and calcium uptake (lower graph) by high-resolution respirometry with the Oroboros Fluo Smart-Module in mitochondria isolated from mouse liver.

Representative trace for calcium uptake protocol (SUIT-035_CaG_D083) as described in Figure 3. Observed in 4 technical repeats with the same preparation of imt. Experiment 2021-06-29 P7-02.

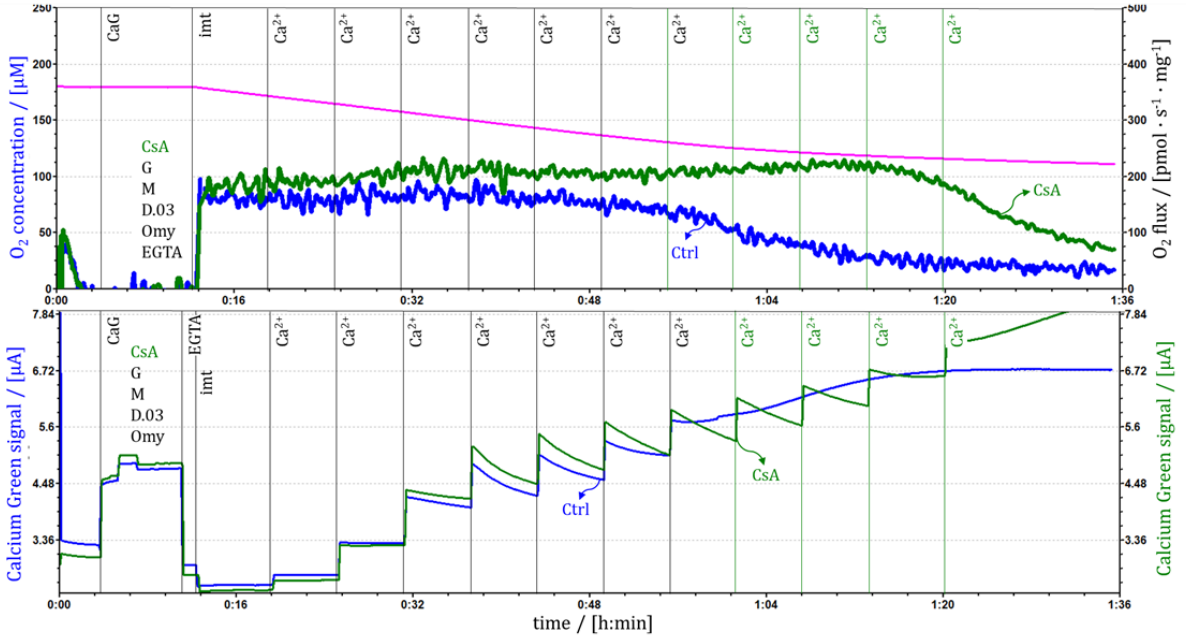


**Figure S10. Irregular patterns in both Ctrl and CsA group in leak respiration.** Simultaneous measurements of respiration (upper graph) and calcium uptake (lower graph) by high-resolution respirometry with the Oroboros Fluo Smart-Module in mitochondria isolated from mouse liver. Representative trace for calcium uptake protocol (SUIT-035_CaG_D083) as described in Figure 3. Observed in 1 experimental run. Experiment 2021-08-12 P1-03.

## Supporting information E

## Statistics for Figure 4

**Table S5. Means ± SD and *p*-values from Figure 4a summarized:** ANOVA one-way and Tukey's multiple comparisons test. Data analyzed by GraphPad10.4.

| | Mean ± SD | CaUC Ctrl | CaUC CsA | CaUC CsA-Ctrl | CaRC Ctrl | CaRC CsA |
|---|---|---|---|---|---|---|
| **CaUC Ctrl** | 122.6 ± 29.22 | - | | | | |
| **CaUC CsA** | 226.1 ± 32.92 | 0.0002⏚ | - | | | |
| **CaUC CsA-Ctrl** | 103.5 ± 10.52 | 0.6984 | 0.0043 | - | | |
| **CaRC Ctrl** | 296 ± 20.47 | 0.0026# | 0.0560 | <0.0001 | - | |
| **CaRC CsA** | 420.5 ± 40.24 | 0.0007 | 0.0018# | 0.0001 | 0.0017⏚ | - |
| **CaRC CsA-Ctrl** | 124.5 ± 23.51 | >0.9999 | 0.0051 | 0.1420# | 0.0002 | <0.0001 |

⏚ CsA effect
# CaUC effect

## Supporting information F

## Influence of ATP on calcium uptake

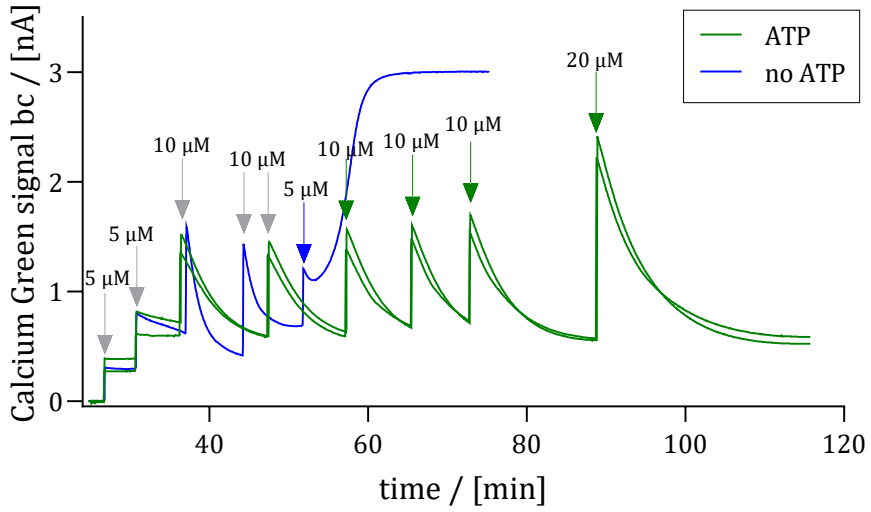


**Figure S11. Influence of ATP on calcium uptake.** ATP 1 mM was added at the beginning of the assay (green lines). The control (blue line) without ATP was performed simultaneously. The arrows indicate calcium titrations, with the specific concentration of each titration above the arrow. Gray arrows represent titrations in all groups, the blue arrow in control and green arrows in the ATP groups. Protocol: CaG; G; M; D(0.03 mM); T(1 mM-optional); Omy(20 nM); EGTA; imt; $Ca^{2+}$*, the graph shows traces only after imt titration. The CaG signal after sample titration was set as zero (mean ± SD: 2.12 ± 0.27 nA). *N* = 1, *n* = 2.

## Supporting information G

## DatLab files used for figures

**Figure 2:** 2021-06-15 P1-03, 2021-06-15 P2-03, 2021-06-23 P3-02, 2021-06-23 P4-02, 2021-06-29 P3-02, 2021-06-29 P4-02, 2021-07-15 P3-02, 2021-07-15 P4-02, 2021-07-20 P3-02, 2021-07-20 P4-02, 2021-08-12 P3-02, 2021-08-12 P4-02, 2021-09-02 P5-02, 2021-09-02 P6-02, 2021-09-09 P1-03, 2021-09-09 P2-02.

**Figure 4 and 5:** 2021-06-29 P1-02, 2021-06-29 P2-02, 2021-06-29 P7-02, 2021-06-29 P8-02, 2021-08-03 PQ1-04, 2021-08-03 PQ2-03, 2021-08-12 P1-03, 2021-08-12 P2-03, 2021-09-02 P3-02, 2021-09-02 P4-02, 2021-09-09 P3-02, 2021-09-09 P4-02, 2021-09-09 PN4-02, 2021-09-09 PN5-02.

**Figure 6:** 2020-12-10 P8-02, 2021-01-21 P8-03, 2021-01-21 P7-03, 2021-02-04 P8-02, 2021-02-17 P8-02, 2021-02-25 P8-02, 2021-03-09 P8-02, 2021-05-10 P8-03.

**Figure 7b:** 2022-05-09 P4-02, 2022-05-10 P4-03, 2022-06-08_XA-002-03, 2022-06-21_XA-002_04, 2024-08-12_XA-003_04.

**Figure S1c:** 2022-01-20 P1-03, 2022-01-20 P2-02, 2021-06-29 P1-03, 2021-06-29 P2-03.

**Figure S1d and S1e:** 2021-03-30 P5-03, 2021-03-30 P5-04, 2021-03-30 P7-03, 2021-03-30 P7-04, 2021-03-30 P8-02, 2021-03-30 P8-03, 2021-04-01 P5-02, 2021-04-01 P5-03, 2021-04-01 P7-02, 2021-04-01 P7-03, 2021-04-01 P8-02, 2021-04-01 P8-03, 2021-04-07 P5-02, 2021-04-07 P5-03, 2021-04-07 P7-02, 2021-04-07 P7-03, 2021-04-07 P8-02, 2021-04-07 P8-03.

**Figure S3:** 2021-06-29 P1-03, 2021-06-29 P2-03, 2021-08-12 P1-04, 2021-08-12 P2-04, 2021-09-02 P3-03, 2021-09-02 P4-04, 2021-09-09 P3-03, 2021-09-09 P4-03

**Figure S4, calibration curves:** 2021-06-29 P1-03, 2021-06-29 P2-03, 2021-06-29 P7-03, 2021-06-29 P8-03, 2021-08-03 PQ1-06, 2021-08-03 PQ2-04, 2021-08-12 P1-04, 2021-08-12 P2-04, 2021-09-02 P3-03, 2021-09-02 P4-04, 2021-09-09 P3-03, 2021-09-09 P4-03, 2021-09-09 PN4-04, 2021-09-09 PN5-04.

**Figure S5:** 2021-02-17 P7-02, 2021-02-17 P8-02, 2021-02-25 P7-02, 2021-02-25 P8-02, 2021-03-09 P7-02, 2021-03-09 P8-02.

**Figure S6:** 2021-02-17 P5-02, 2021-02-25 P5-02, 2021-03-09 P5-02.

**Figure S7:** 2021-03-22 P8-02, 2021-03-24 P8-02.

**Figure S11:** 2021-03-22 P5-02, 2021-03-22 P6-02, 2021-03-22 P7-02, 2021-03-22 P8-02.